π-Conjugated Nanohoops: A new generation of curved materials for organic electronics

Rupam Roy, Clément Brouillac, Emmanuel Jacques, Cassandre Quinton, Cyril Poriel

▶ **To cite this version:**

Rupam Roy, Clément Brouillac, Emmanuel Jacques, Cassandre Quinton, Cyril Poriel. π-Conjugated Nanohoops: A new generation of curved materials for organic electronics. Angewandte Chemie International Edition, 2024, 63 (30), pp.e202402608. 10.1002/anie.202402608 . hal-04596481

HAL Id: hal-04596481
https://hal.science/hal-04596481v1

Submitted on 30 Oct 2024

HAL is a multi-disciplinary open access archive for the deposit and dissemination of scientific research documents, whether they are published or not. The documents may come from teaching and research institutions in France or abroad, or from public or private research centers.

L'archive ouverte pluridisciplinaire **HAL**, est destinée au dépôt et à la diffusion de documents scientifiques de niveau recherche, publiés ou non, émanant des établissements d'enseignement et de recherche français ou étrangers, des laboratoires publics ou privés.

Distributed under a Creative Commons Attribution - NonCommercial - NoDerivatives 4.0 International License

How to cite: *Angew. Chem. Int. Ed.* **2024**, e202402608
doi.org/10.1002/anie.202402608

Cycloparaphenylenes

π-Conjugated Nanohoops: A New Generation of Curved Materials for Organic Electronics

Rupam Roy, Clément Brouillac, Emmanuel Jacques, Cassandre Quinton, and Cyril Poriel**

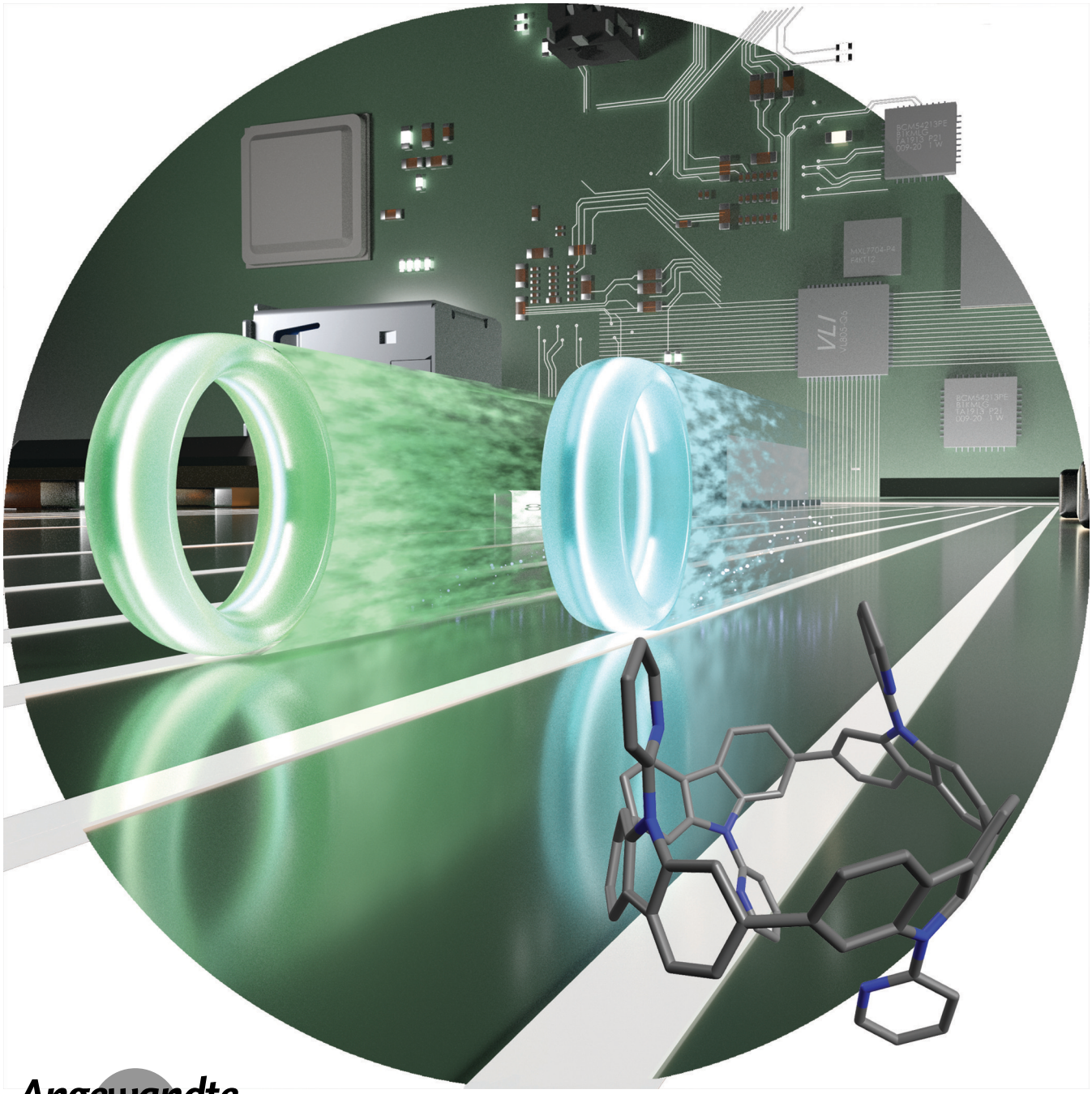

© 2024 The Authors. Angewandte Chemie International Edition published by Wiley-VCH GmbH

Abstract: Nanohoops, cyclic association of π-conjugated systems to form a hoop-shaped molecule, have been widely developed in the last 15 years. Beyond the synthetic challenge, the strong interest towards these molecules arises from their radially oriented π-orbitals, which provide singular properties to these fascinating structures. Thanks to their particular cylindrical arrangement, this new generation of curved molecules have been already used in many applications such as host–guest complexation, biosensing, bioimaging, solid-state emission and catalysis. However, their potential in organic electronics has only started to be explored. From the first incorporation as an emitter in a fluorescent organic light emitting diode (OLED), to the recent first incorporation as a host in phosphorescent OLEDs or as charge transporter in organic field-effect transistors and in organic photovoltaics, this field has shown important breakthroughs in recent years. These findings have revealed that curved materials can play a key role in the future and can even be more efficient than their linear counterparts. This can have important repercussions for the future of electronics. Time has now come to overview the different nanohoops used to date in electronic devices in order to stimulate the future molecular designs of functional materials based on these macrocycles.

1. Introduction

Cyclo-*para*-phenylenes (CPPs) are hoop-shaped macrocycles, constituted of 1,4-linked phenyl rings (*para* substitution), with radially oriented π-orbitals. They are the flagship molecules of the family of nanohoops also called nanorings,[1–3] and are considered as the simplest segment of armchair carbon nanotubes (CNTs).[4–10] The chemistry of CPPs was first conceptualized by Parekh and Guha in 1934,[11] and, after 60 years, Vögtle tried to innovate a synthetic route for CPPs.[12] Unfortunately, all their attempts were unsuccessful. The synthesis of these nanohoops was a great challenge because of the large strain energy adopted by non-planar phenyl rings. However, those preliminary works laid the foundation for the first synthesis of **[n]CPPs** by Jasti and Bertozzi in 2008 (n denotes the number of repetating units). They reported the first synthesis of **[9]**, **[12]** and **[18]CPPs**: *"carbon nanohoops"* were born.[1] Then, the chemistry of nanohoops has been more and more studied thanks to the pioneering contributions from leading groups of Jasti,[1,6] Itami,[2] Yamago,[3] and Isobe,[13] followed by many other groups.[14–30] Various directions have been taken to explore the possible applications of nanohoops[31–37] and one of these emerging applications was organic electronic technologies. Organic electronics has encountered a tremendous development in the last 30 years and represents nowadays one important branch of electronic.[38,39] The first question to address herein is *'Why using nanohoops in electronics'?* The answer is manifold. The first aspect is linked to their very uncommon electronic properties reported, over the years, by the groups involved in this field. The unusual properties of the nanohoops have emerged as a consequence of cyclic association of their building units and particularly their radially-oriented π-orbitals. The size-dependence photophysical and electrochemical properties of these highly strained structures was surely one of the most exciting.[28,31,40–53] For example, most of CPP derivatives exhibit a common absorption maximum nearby 340 nm and their extinction coefficient depicts a little enhancement with increase of nanohoop size.[31,40–43] On moving from smaller to larger nanohoops, most of nanohoops demonstrate a hypsochromic shift in emission along with increase in fluorescence quantum yield Φ_F,[28,31,40–49] and increase of the gap between the highest occupied molecular orbital (HOMO) and the lowest unoccupied molecular orbital (LUMO).[40–43,51] Thus, **[12]CPP** is highly emissive in solution ($\Phi_F = 0.66–0.89$[42–44]) and, on contrary, **[5]CPP** is not emissive.[54] The bright emissive behaviour of large CPPs has been interpreted as a consequence of a high reorganization at the excited state which is impossible in the small highly strained nanohoops.[55] The emission blue shift and the enlargement of HOMO–LUMO gap with increasing CPPs size appear to be significantly different than those of their linear congeners (i.e. *para*-substituted phenyl oligomers). Indeed, the linear oligo-*para*-phenylenes show a gradual red shift of absorption and emission in line with a decrease of the HOMO–LUMO gap when the number of phenyl units increases.[56] Considering that linear π-conjugated systems are the molecular pillars which have allowed the development of organic electronics,[38] studying their cyclic counterparts appears as an exciting challenge. This emission blue shift as the size of the CPP increases has been then described for other families of nanohoops built with fluorenes,[47] carbazoles[48] or naphthalenes.[57] Thus, designing nanohoops gives access to new organic semi-conductors (OSCs) displaying different ranges of HOMO–LUMO gap, absorption and emission compared to their linear analogs and to a different evolution of their electronic properties as a function of their size.

[*] Dr. R. Roy, Dr. C. Brouillac, Dr. C. Quinton, Dr. C. Poriel
Univ Rennes, CNRS, ISCR-UMR CNRS 6226, F-35000 Rennes
France
E-mail: Cyril.poriel@univ-rennes.fr
cassandre.quinton@univ-rennes.fr
Dr. R. Roy
Department of Chemistry
University of Florida
Gainesville, Florida, United States, 32603
Dr. E. Jacques
Univ Rennes, CNRS, IETR-UMR CNRS 6164, F-35000 Rennes,
France

© 2024 The Authors. Angewandte Chemie International Edition published by Wiley-VCH GmbH. This is an open access article under the terms of the Creative Commons Attribution Non-Commercial NoDerivs License, which permits use and distribution in any medium, provided the original work is properly cited, the use is non-commercial and no modifications or adaptations are made.

15213773, 0, Downloaded from https://onlinelibrary.wiley.com/doi/10.1002/anie.202402608 by Université De Rennes, Wiley Online Library on [08/07/2024]. See the Terms and Conditions (https://onlinelibrary.wiley.com/terms-and-conditions) on Wiley Online Library for rules of use; OA articles are governed by the applicable Creative Commons License

Besides their uncommon (and difficult to predict) electronic properties, the cyclic and curved architectures of nanohoops are intrinsically interesting. It has been shown that the solubility in organic solvents is high[58–61] due to the decrease of the intermolecular π-π stacking interactions. The cyclic nature can also significantly modify π–π interactions in the solid state and the resulting packing arrangement compared to linear analogues and these characteristics can be interestingly used in electronic devices. In addition, due to their cyclic nature, the nanohoops are devoid of end groups,[30,62,63] which usually cause excitons trapping and thus, diminish the effective charge migration, as seen in linear derivatives. Considering the huge development of fullerene-based materials for electronic applications,[64,65] in the last thirty years, studying new generations of curved materials appeared highly exciting.

Despite the impressive development of organic electronics in the last decade and the thousands of OSCs used as active layers in the three main electronic devices, either Organic Light-Emitting Diodes (OLEDs), Organic Field-Effect Transistors (OFETs) or Organic PhotoVoltaics (OPVs), the examples of nanohoops incorporations have remained extremely rare. This is surely due to the difficulty to synthesize, at the beginning of the field, nanohoops in large quantities. However, the impressive progresses made in term of synthetic approaches have recently allowed to incorporate nanohoops in electronic devices and even to optimize their performance,[66] which is a key feature to reach a high efficiency. Some of these examples have clearly highlighted the interest of such a type of structures for future electronic devices based on curved materials. The present work aims to discuss all these examples and shows how nanohoops went from a laboratory curiosity to functional materials enabling high-performance devices. However, this field of *nanohoops in electronics* is still in its infancy and the goal of this review is to provide to molecular chemists all the tools to design the future very high efficiency nanohoop-based materials.

2. Theoretical Insights into Charge Transport Properties of Nanohoops

The unconventional intermolecular packing in solid-state reported over the years for CPPs[42] has first motivated theoretical studies on charge transport. Indeed, before the synthesis of nanohoops has made considerable progresses allowing their incorporation in organic electronic devices, it was particularly important to theoretically envisage their charge transport.

In 2017, Guo, Yan *et al.* theoretically predicted the nature of electron transport for **[n]CPPs** ($n=5$, 6, 8, 10, Figure 1), by configuring a virtual molecular device using non equilibrium Green's function in combination with density functional theory.[67] They selectively chosed **[6]CPP** and linear carbon atomic chains acting as electrodes. Introduction of linear chains minimized the complexity emanating from direct electrode-molecule contact. The computational results have revealed that the negative differential reflectance (NDR) phenomenon was found in **[6]CPP**-electrode configuration. The electron transport property of **[6]CPP** was ascribed to an effective electronic coupling between nanohoop core and side chain carbon electrodes. Noteworthy, other sizes of **[n]CPPs** ($n=5$, 8 and 10), along with N-atom doped **[6]CPP** (**N[6]CPP** (**1**), Figure 1), exhibited the same NDR characteristics. The authors have also demonstrated that the substitution of carbon chain electrodes by Au cluster electrodes also resulted in emergence of NDR phenomenon, evidencing that this characteristic is an inherent feature for CPPs.

In 2019, Houk, Yavuz and co-workers unveiled the correlation of charge transport parameters (electronic coupling J, reorganization energy λ, energetic disorder σ and hole mobility μ^h) with the hoop size, for a series of **[n]CPPs** ($n=5$–12, Figure 1), by molecular dynamics and charge transport dynamics simulation.[30] As the mobility is driven by the reorganization energy λ (energetic disorder being similar for all the CPPs investigated), this parameter is of key importance for charge transport properties. As the CPP size increases, the reorganization energy decreases ($\lambda=$ 457 meV and 173 meV for **[5]CPP** and **[12]CPP**, respec-

Cassandre Quinton is a CNRS researcher at the University of Rennes working in the field of π-conjugated materials. She received her Ph.D. in Chemistry from the Ecole Normale Supérieure (Paris-Saclay, France). After that, she obtained a postdoctoral fellowship from the Japan Society for the Promotion of Science to conduct her research at the Nara Institute of Science and Technology. In 2016, she was awarded a Marie Skłodowska-Curie Individual Fellowship to start her research on hoop-shaped π-conjugated macrocycles, i.e. nanohoops, at the University of Rennes. In 2018, she joined the CNRS. Her current molecules of interest are cyclic bridged oligo-para-phenylenes.

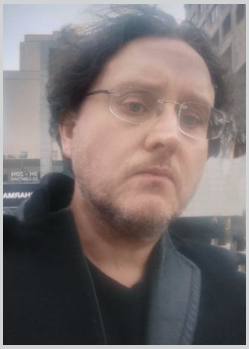

Cyril Poriel is CNRS Research Director at Institut des Sciences Chimiques de Rennes- (Rennes University, France). His main research interest deals with the design of π-conjugated molecular architectures for Organic Electronics. He is particularly interested in the design of blue emitting fluorophores for OLEDs, high triplet host materials for phosphorescent OLEDs and nanohoops.

© 2024 The Authors. Angewandte Chemie International Edition published by Wiley-VCH GmbH

15213773, 0, Downloaded from https://onlinelibrary.wiley.com/doi/10.1002/anie.202402608 by Université De Rennes, Wiley Online Library on [08/07/2024]. See the Terms and Conditions (https://onlinelibrary.wiley.com/terms-and-conditions) on Wiley Online Library for rules of use; OA articles are governed by the applicable Creative Commons License

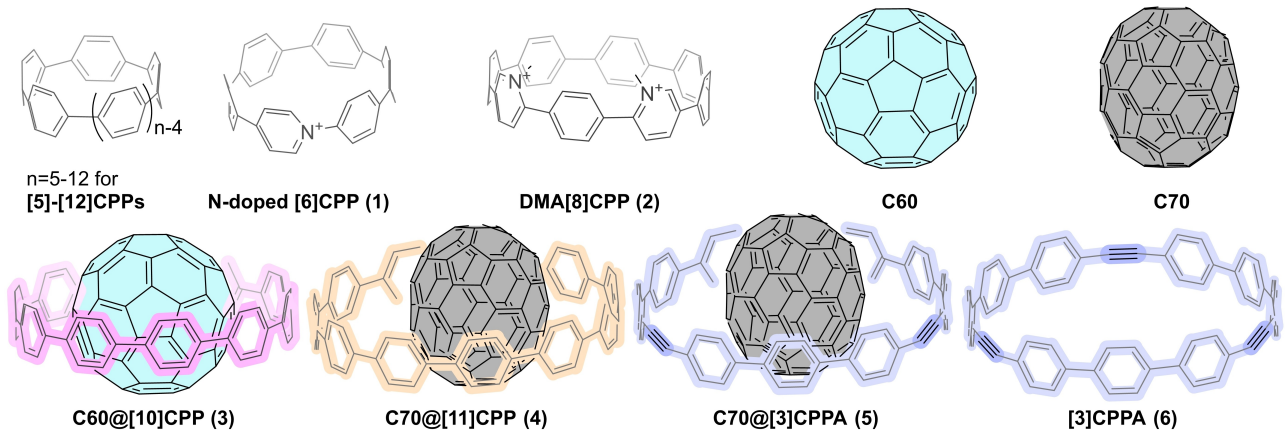

Figure 1. Chemical structures of the nanohoops discussed in section 2.

tively, Table 1). The depletion of reorganization energy and electronic coupling with enlargement of the size is ascribed to the increase of charge delocalization over the whole framework of larger CPPs. Structural rigidity of small CPPs makes them more resistant to structural deformations, also participating to their high reorganization energy. In order to determine the mobility for different CPPs, kinetic Monte Carlo simulation was conducted disclosing that the mobility dramatically increased with the hoop size. The evolution of μ follows $\mu \sim n^4$. The charge carrier mobility value was evaluated at $\mu = 7.2\times10^{-2}\,cm^2\,V^{-1}\,s^{-1}$ for **[5]CPP**, which is significantly increased to $183\times10^{-2}\,cm^2\,V^{-1}\,s^{-1}$ for **[12]CPP** (Table 1). Finally, the authors proposed that CPPs are less impacted by structural and energetic disorder than their linear oligophenylene counterparts due to their lack of end groups.

The above theoretical investigations have shown how hoop size influences the charge transport parameters for a series of CPPs, the simplest version of nanohoops. The same year, the groups of Negri and Sancho-Garcia report their investigations on the effect of incorporation of acceptor unit within a CPP on reorganization energy and electronic coupling of different nanohoops.[68] The idea was to investigate how reorganization energy and electronic coupling can be modulated in a nanohoop by the introduction of an acceptor fragment. Thus, *N*,*N*-dimethylaza[8]cyclo-*para*-phenylene (**DMA[8]CPP** (**2**), Figure 1) was compared to **[8]CPP**. For **[8]CPP**, the authors have shown that the oxidized/reduced forms have similar structures with a reduced twisting of phenyl units, compared to the neutral form. Compound **2** displayed a different behaviour with a significant structural modification centred on the donor (phenyl) or acceptor (*N*-methyl pyridinium) units for the oxidized/reduced forms, respectively. The reorganization energies linked to their structural modifications have been calculated, showing that the incorporation of acceptor unit increases λ for the oxidation and decreases λ for the reduction compared to **[8]CPP**. Of particular interest, the authors have calculated similar reorganization energies for p-type and n-type charge transport, both close to 300 meV, signing an ambipolar behaviour, of great interest for organic electronics. Moreover, unlike most planar OSCs, where the layer in which the molecules are herring-bone arranged identifies the high-mobility plane, both **[8]CPP** and **DMA-[8]CPP** (**2**) displayed more efficient inter-layer charge transport than the intra-layer charge transport. This is a key characteristic for future designs.

In 2019 as well, Yavuz and co-workers report another computational approach, elucidating the importance of host–guest complexation in the electronic device

Table 1: Selected theoretical data for nanohoops discussed in section 2.

Nanohoops	J/meV	λ/meV	σ/meV	μ^h/cm^2 V^{-1} s^{-1}
[5]CPP	*a*	457	66	7.2×10^{-2}
[6]CPP	*a*	391	49	5.6×10^{-2}
[7]CPP	*a*	304	48	28×10^{-2}
[8]CPP	*a*	260	45	24×10^{-2}
[9]CPP	*a*	240	49	48×10^{-2}
[10]CPP	*a*	211	42	112×10^{-2}
[11]CPP	*a*	196	52	107×10^{-2}
[12]CPP	*a*	173	45	183×10^{-2}
3	9.4	231	63	1.9×10^{-2}
4	22	203	43	27×10^{-2}
5	11	179	125	0.21×10^{-2}

[a] Electronic coupling (J) of **[5–12]CPP** = 1–10 meV, λ = reorganization energy, σ = energetic disorder and μ^h = hole mobility.

© 2024 The Authors. Angewandte Chemie International Edition published by Wiley-VCH GmbH

15213773, 0, Downloaded from https://onlinelibrary.wiley.com/doi/10.1002/anie.202402608 by Université De Rennes, Wiley Online Library on [08/07/2024]. See the Terms and Conditions (https://onlinelibrary.wiley.com/terms-and-conditions) on Wiley Online Library for rules of use; OA articles are governed by the applicable Creative Commons License

performance.[69] They investigated charge transport for three types of circular non-covalently attached Donor-Acceptor (D–A) systems, with "Saturn-like" arrangement, namely **C60@[10]CPP** (**3**), **C70@[11]CPP** (**4**), and **C70@[3]CPPA** (**5**), as shown in Figure 1 (**[3]CPPA** (**6**) represents [3]-cyclo-*para*-phenyleneacetylene nanohoop). Herein, nanohoop and fullerene act as electron donor and acceptor, respectively. Note that the three systems investigated are 1:1 complexes. The solid-state packing, which is the key parameter involved in charges transport, was different for **[10–11]CPPs** and **[3]CPPA** based systems. A contorted network was identified for both **C60@[10]CPP** (**3**) and **C70@[11]CPP** (**4**) complexes, which changed to columnar packing to create 3D brickwork-like network in the case of **C70@[3]CPPA** (**5**). As a result of the different packing arrangements, the hole mobility (μ^h) for the three donor materials was predicted different. From kinetic Monte Carlo simulation, the values obtained were: $\mu^h = 1.9\times10^{-2}$, 27×10^{-2} and $0.21\times10^{-2}\,cm^2V^{-1}s^{-1}$ for **3**, **4** and **5**, respectively, Table 1. Despite the weak reorganization energy of donor **[3]CPPA** in **5** compared to the CPPs in the complexes **3** and **4**, this host/guest compound displays the lowest hole mobility because of a large energetic disorder. On the same line, the electron mobility of **C70**, when complexed in **4** and **5**, is significantly higher than that of **C60** in **3** (521 and 6000 times respectively). This enhanced mobility for **C70** complex is due to close intermolecular contacts between **C70** and nanohoop as well as shorter distance between adjacent **C70** pairs. The photovoltaic properties of the three complexes were also evaluated by designing virtual devices, comprised of indium tin oxide (ITO)/fullerene@nanohoop/Al configuration, showing power conversion efficiency (PCE) values of 2.8%, 9.8%, and 9.0% for **C60@[10]CPP** (**3**), **C70@-[11]CPP** (**4**), and **C70@[3]CPPA** (**5**), respectively. Reaching virtual PCE values nearby 10% appeared as a noteworthy result and this work was an important theoretical finding on the use of nanohoops in OPV, although the authors also noted the lack of polycrystallinity of these compounds.

3. Applications of Nanohoops in Organic Electronic Devices

A table gathering selected electronic properties of nanohoops is provided (Table 2).

3.1. Incorporation in OLED Devices

Of all the building blocks used to design OSCs, the fluorene fragment holds a particular place due notably to its fluorescence properties. As its chemistry has strongly contributed to the development of OLEDs,[70–74] the fluorene fragment has been rapidly considered as building unit in nanohoops. In 2015, Yamago and co-workers have reported the first examples of cyclofluorenes with a cylinder shape but no device was reported.[75] In 2016, Huang and co-workers also developed a highly-strained (E_{strain} = 79.8 kcal/mol) fluorene-based nanohoop, namely [4]cyclo-9,9-dipropyl-2,7-fluorene (**[4]CF** (**7**), Figure 2 top).[22] The nanohoop was synthesized via formation of relaxed tetra-platinum complexes intermediate, according to the synthetic protocol reported by Yamago[3] and modified by Isobe.[13] They managed to obtain the desired fluorene-based nanohoop **7** in a yield of 14% along with its corresponding linear tetrafluorene analogue **[4]LF** (**8**) (yield: 25%, see structure in Figure 2 middle). The X-ray structure revealed that **7** contained an ellipsoid cavity, and that fluorene moieties displayed an out-of-plane distortion (average distance between the 2 and 7 sites of 6.65 *vs* 6.80–6.90 Å in classical planar fluorene). This distortion can, obviously, not be observed in its linear analogue **8**. The herringbone structure of **7** displayed C–H···π and π···π interactions. In emission spectroscopy, **7** showed a green fluorescence in tetrahydrofuran THF (λ^f_{max} = 512 nm), while its linear analogue **8** displayed a blue emission (λ^f_{max} = 406 nm). Investigating the differences between cyclic and linear oligophenylenes is, in this research field, a very relevant consideration, which have highlighted over the years the peculiar properties of nanohoops induced by their curvature.[22,23,62,63,76–78] Herein, Huang and co-workers proposed that **7** is emissive despite a forbidden HOMO→LUMO transition (as classically observed for nanohoops) thanks to conformational distortion-induced geometrical relaxation in Frank Condon state or self-trapping of lower excited state. Finally, keeping in mind the high solution processability of **7**, an OLED device was fabricated using spin-coated techniques, with **7** as fluorescent emitter. The device architecture was: ITO/PEDOT:PSS/**7**/TPBi/LiF/Al with PEDOT:PSS meaning

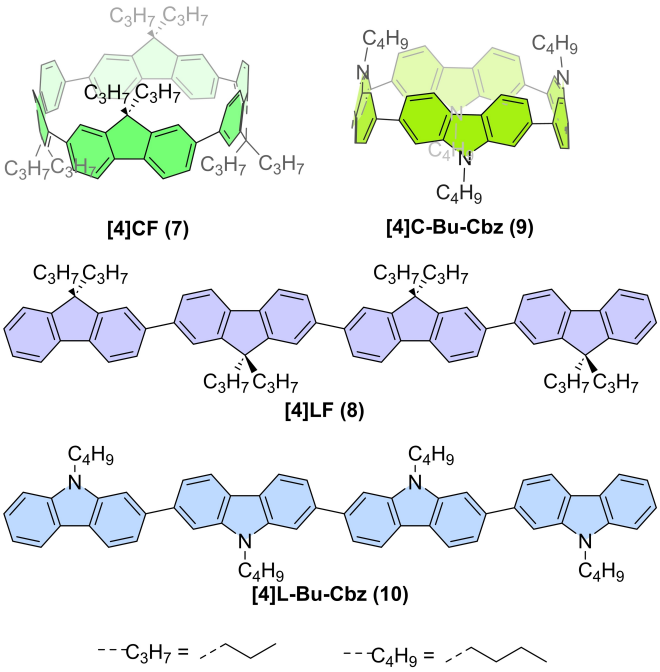

Figure 2. Cyclic tetrafluorene **[4]CF** (**7**) and tetracarbazole **[4]C-Bu-Cbz** (**9**) (top) and their linear analogues **[4]LF** (**8**) (middle) and **[4]L-Bu-Cbz** (**10**) (bottom).

© 2024 The Authors. Angewandte Chemie International Edition published by Wiley-VCH GmbH

15213773, 0, Downloaded from https://onlinelibrary.wiley.com/doi/10.1002/anie.202402608 by Université De Rennes, Wiley Online Library on [08/07/2024]. See the Terms and Conditions (https://onlinelibrary.wiley.com/terms-and-conditions) on Wiley Online Library for rules of use; OA articles are governed by the applicable Creative Commons License

Table 2: Summary of electronic properties and device performance.

Compound	λ^{abs}_{max}/nm[a] (solvent)	λ^{f}_{max}/nm[b] (solvent)	Φ_F (solvent)	λ^{P}_{max}/nm (solvent)[c]	E_{HOMO}/eV[d]	E_{LUMO}/eV[d]	E_{gap}/eV[e]	Device characteristics[f]	Ref.
7	349 (THF)	512 (THF)	0.45 (THF)	—	−5.35	−2.35	3.00	Luminance = 878 cd cm^{-2} CE_{max} = 0.83 cd A^{-1}	Huang, 2016[22]
9	337 (C_6H_{12})	483 (C_6H_{12})	0.20 (C_6H_{12})	548 (2–MeTHF)	−5.18	−2.40	2.78	EQE_{max} = 17 %; CE_{max} = 20.6 cd A^{-1}; PE_{max} = 25.8 lm W^{-1}; $\mu^{h}_{FET_sat}$ = 1.0×10^{-5} cm^{2}V^{-1}s^{-1}; $\mu^{h}_{FET_lin}$ = 1.0×10^{-5} cm^{2}V^{-1}s^{-1}; μ^{h}_{SCLC} = 2.8×10^{-4} cm^{2}V^{-1}s^{-1}	Poriel, 2021[66,129]
10	367 (C_6H_{12})	403 (C_6H_{12})	0.82 (C_6H_{12})	520 (2–MeTHF)	−5.30	−2.17	3.13	EQE_{max} = 11.1 %; CE_{max} = 13.0 cd A^{-1} PE_{max} = 15.7 lm W^{-1} $\mu^{h}_{FET_sat}$ = 1.1×10^{-4} cm^{2}V^{-1}s^{-1} $\mu^{h}_{FET_lin}$ = 3.5×10^{-5} cm^{2}V^{-1}s^{-1} μ^{h}_{SCLC} = 1.5×10^{-4} cm^{2}V^{-1}s^{-1}	Poriel, 2023[66]
11	331 (toluene)	508 (toluene)	0.34 (toluene)	600 (toluene)	−5.49	−1.88	3.61	EQE_{max} = 1.0 %	Zysman-Colman, 2023[109]
12	~335 [g]	–	–	–	−5.39	−3.87	1.52	PCE = 3.3 %; J_{sc} = 9.2 mA cm^{-2} $\mu^{e}_{FET_sat}$ = 1.5×10^{-3} cm^{2}V^{-1}s^{-1}	Nuckolls, 2016[63]
13	~310[g]	–	–	–	−5.69	−3.90	1.79	PCE = 3.5 %; J_{sc} = 9.8 mA cm^{-2} $\mu^{e}_{FET_sat}$ = 1.5×10^{-3} cm^{2}V^{-1}s^{-1}	Nuckolls, 2016[63]
14	~407[g]	–	–	–	−5.45	−3.86	1.59	PCE = 1.1 %; J_{sc} = 4.2 mA cm^{-2} $\mu^{e}_{FET_sat}$ = 2.3×10^{-4} cm^{2}V^{-1}s^{-1}	Nuckolls, 2016[63]
15	~314[g]	–	–	–	−5.75	−3.86	1.89	PCE = 0.73 %; J_{sc} = 3.2 mA cm^{-2} $\mu^{e}_{FET_sat}$ = 1.9×10^{-5} cm^{2}V^{-1}s^{-1}	Nuckolls, 2016[63]
16	~400[g]	~600 [g]	–	–	–	−3.82	–	$\mu^{e}_{FET\_sat}$ = 4.1×10^{-3} cm^{2}V^{-1}s^{-1}	Nuckolls, 2018[116]
17	~400[g]	~580 [g]	–	–	–	−3.80	–	$\mu^{e}_{FET\_sat}$ = 9.9×10^{-4} cm^{2}V^{-1}s^{-1}	Nuckolls, 2018[116]
18								PCE = 8.0 %; J_{sc} = 15.24 mA.cm^{-2}	Tao, 2020[125]
19								PCE = 10.5 %; J_{sc} = 19.27 mA.cm^{-2} μ^{h} = 1.52×10^{-3} cm^{2}V^{-1}s^{-1} μ^{e} = 1.57×10^{-3} cm^{2}V^{-1}s^{-1}	Tao, 2020[125]
20	345 ($CHCl_3$)	477 ($CHCl_3$)	0.59 ($CHCl_3$)	–	−5.99 [h]			μ^{e}_{SCLC} = 4.5×10^{-6} cm^{2}V^{-1}s^{-1}	Yamago, 2017[127]
25	337 (C_6H_{12})	486 (C_6H_{12})	0.19 (C_6H_{12})	–	−5.17	−2.22	2.95	$\mu^{h}_{FET\_sat}$ = 1.0×10^{-5} cm^{2}V^{-1}s^{-1} $\mu^{h}_{FET_lin}$ = 0.97×10^{-5} cm^{2}V^{-1}s^{-1} μ^{h}_{SCLC} = 2.7×10^{-4} cm^{2}V^{-1}s^{-1}	Poriel, 2019[128,129]
26	337 (C_6H_{12})	482 (C_6H_{12})	0.20 (C_6H_{12})	–	−5.19	−2.21	2.98	$\mu^{h}_{FET\_sat}$ = 8.8×10^{-6} cm^{2}V^{-1}s^{-1} $\mu^{h}_{FET_lin}$ = 2.6×10^{-6} cm^{2}V^{-1}s^{-1} μ^{h}_{SCLC} = 1.4×10^{-4} cm^{2}V^{-1}s^{-1}	Poriel, 2021[129]
28	342 (C_6H_{12})	432, 456 (C_6H_{12})	0.56 (C_6H_{12})	–	−5.22	−2.51	2.71	$\mu^{h}_{FET\_sat}$ = 4.2×10^{-5} cm^{2}V^{-1}s^{-1} $\mu^{h}_{FET_lin}$ = 9.3×10^{-6} cm^{2}V^{-1}s^{-1} μ^{h}_{SCLC} = 7.7×10^{-5} cm^{2}V^{-1}s^{-1}	Poriel, 2023[48]
29	~344 (CH_2Cl_2)	476 (CH_2Cl_2)	0.25 (CH_2Cl_2)	–	–	–	–	μ^{e}_{SCLC} = 1.4×10^{-4} cm^{2}V^{-1}s^{-1}	Du, 2021[134]
30	371 (CH_2Cl_2)	510 (CH_2Cl_2)	0.15 CH_2Cl_2)	–	–		–	μ^{e}_{SCLC} = 1.8×10^{-4} cm^{2}V^{-1}s^{-1}	Du, 2021[134]
31	356 (CH_2Cl_2)	479 (CH_2Cl_2)	0.019 (CH_2Cl_2)	–	–	–	–	μ^{h}_{SCLC} = 9.49×10^{-6} cm^{2}V^{-1}s^{-1} μ^{e}_{SCLC} = 1.82×10^{-4} cm^{2}V^{-1}s^{-1}	Du, 2022[135]
[8]CPP	333 (C_6H_{12})	528 (C_6H_{12})	0.25 (C_6H_{12})	671 (EEET [i])	−5.28	−2.60	2.68	$\mu^{h}_{FET\_sat}$ = n.m.[j] ; $\mu^{h}_{FET\_lin}$ = n.m.[j] μ^{h}_{SCLC} = 1.2×10^{-7} cm^{2}V^{-1}s^{-1}	Poriel, 2023[48] Yamago, 2014[83]

© 2024 The Authors. Angewandte Chemie International Edition published by Wiley-VCH GmbH

15213773, 0, Downloaded from https://onlinelibrary.wiley.com/doi/10.1002/anie.202402608 by Universite De Rennes, Wiley Online Library on [08/07/2024]. See the Terms and Conditions (https://onlinelibrary.wiley.com/terms-and-conditions) on Wiley Online Library for rules of use; OA articles are governed by the applicable Creative Commons License

Table 2: (Continued)

Compound	λ^{abs}_{max}/nm[a] (solvent)	λ^{f}_{max}/nm[b] (solvent)	Φ_F (solvent)	λ^{p}_{max}/nm (solvent)[c]	E_{HOMO}/eV[d]	E_{LUMO}/eV[d]	E_{gap}/eV[e]	Device characteristics[f]	Ref.
[10]CPP	335/339 (C_6H_{12}/toluene)	464/470 (C_6H_{12}/toluene)	0.59/0.77 (C_6H_{12}/toluene)	610 (EEET[i])	−5.50	−2.51	3.00	$\mu^{h}_{FET\_sat}$ = n.m.[j]; $\mu^{h}_{FET\_lin}$ = n.m.[j] μ^{h}_{SCLC} = 1.1×10^{-8} $cm^2V^{-1}s^{-1}$	Poriel, 2023[48] Zysman-Colman, 2023[109] Yamago, 2014[83]
35	335 (CH_2Cl_2)	490 (CH_2Cl_2)	0.18 (CH_2Cl_2)	–	−5.38	−2.38	3.00	$\mu^{h}_{FET\_lin}$ = 7×10^{-7} $cm^2.V^{-1}.s^{-1}$ $\mu^{h}_{FET\_sat}$ = 3.4×10^{-6} $cm^2.V^{-1}.s^{-1}$	Poriel,Quinton, 2024[138]
36	330 (CH_2Cl_2)	495 (CH_2Cl_2)	0.17 (CH_2Cl_2)	–	−5.32	−2.44	2.88	$\mu^{h}_{FET\_lin}$ = 1.2×10^{-8} $cm^2.V^{-1}.s^{-1}$ $\mu^{h}_{FET\_sat}$ = 2.5×10^{-8} $cm^2.V^{-1}.s^{-1}$	Poriel,Quinton, 2024[138]

a. Wavelength of maximal absorbance, b. Wavelength of maximal fluorescence at room temperature, c. Wavelength of maximal phosphorescence at 77 K, d. Determined from electrochemical data (unless otherwise specified), e. E_{LUMO}-E_{HOMO}, f. CE_{max}: maximal current efficiency, EQE_{max}: maximal external quantum efficiency, PE_{max}: maximal power efficiency, J_{sc}: short-circuit current density; μ^{e}: electron mobility, μ^{h}: hole mobility, μ_{FET_sat}: field effect mobility in the saturated regime, μ_{FET_lin}: field effect mobility in the linear regime, μ_{SCLC}: space-charge-limited current SCLC transport, g. solvent not precised, h. Determined from the ionization potential measured by an atmospheric photoelectron spectrophotometer, i. 2 : 2 : 1 : 1 mixture of ethyl iodide, ether, ethanol, and toluene, j. not measurable.

poly(3,4-ethylenedioxythiophene)-poly(styrenesulfonate) and TPBi (1,3,5-tris(1-phenyl-1H-benzimidazol-2-yl)benzene) used as hole-transporting layer and as electron-transporting layer respectively. **7**-Based OLED exhibited a maximum luminance of 878 cd cm^{-2} and maximum current efficiency (CE) of 0.83 cd A^{-1} in green region. However, the effect of the curvature on the device performance was not highlighted in this work as no comparison was performed with its linear analogue. This was the first example of integration of a nanohoop in an OLED device. Other nanohoops constructed on the assembly of four fluorene fragments have also been reported, showing interesting electronic properties.[23,47,75] Despite low device performance, this work has undoubtedly motivated our group to go deeper in this field and one of our goals was to design a high-efficiency nanohoop for OLED applications.

Linear carbazole-based OSCs have been widely studied in organic electronics, notably due to their strong electron-rich character.[79] This appealing property has been used by our group to design cyclic tetracarbazoles for OLEDs.[66] Note that the first cyclo-2,7-carbazole nanohoops have been reported in 2016 by Yamago and co-workers without nevertheless any incorporation in device.[80] Thus, in 2023, our group has reported the first incorporation of a nanohoop, namely [4]cyclo-*N*-butyl-2,7-carbazole (**[4]C-Bu-Cbz** (**9**), Figure 2 top), in a phosphorescent OLED (PhOLED).[66] As above mentioned, nanohoops have remained almost unexplored in organic electronics due to the difficulty to reach sufficient amounts for device fabrication and optimization. Indeed, to reach high-performance PhOLEDs, a set of optimizations should always be performed such as investigating different electrodes or functional interlayers in the device or different ratio of the phosphorescent emitter in the emissive layer.[81] The recent progresses in terms of synthesis have started to change the deal and have contributed to our advances in nanohoops-based organic devices. This synthetic development will surely allow nanohoops to go one-step further in term of applications. Thus, a large-scale synthesis (1 g of starting 2,7-dipinacol carbazole precursor) of **[4]C-Bu-Cbz** (**9**) was performed with an excellent yield of 58 %. In order to investigate the effect of curvature in PhOLEDs, linear analogue **[4]L-Bu-Cbz** (**10**) was also synthesized (Figure 2 bottom). Interestingly, the nanohoop **9** displays a phosphorescence band at 548 nm (τ_P = 0.65 s) in 2-MeTHF at 77 K, whereas the one of its linear analogue **10** was observed at 520 nm (τ_P = 2.85 s, Figure 3a–b). The triplet state energy E_T of nanohoop **9** (E_T = 2.26 eV) was therefore lower than that of its linear counterpart **10** (E_T = 2.38 eV), showing the key role played by the hoop strain on the reduction of the E_T. As the E_T of both tetracarbazoles were higher than commonly used red phosphorescent emitter $Ir(MDQ)_2(acac)$ (E_T = 2.02 eV, MDQ stands for 2-methyldibenzo[f,h]quinoxaline),[82] they were successfully employed as host materials in red-emitting PhOLEDs.[66] Remarkably, $Ir(MDQ)_2(acac)$ embedded device incorporating **9** as host demonstrated a higher performance than that using its linear analogue **10** (Figure 3c–d). The maximal external quantum efficiency (EQE_{max}), current and power efficiency values (CE_{max} and PE_{max}) were

© 2024 The Authors. Angewandte Chemie International Edition published by Wiley-VCH GmbH

15213773, 0, Downloaded from https://onlinelibrary.wiley.com/doi/10.1002/anie.202402608 by Université De Rennes, Wiley Online Library on [08/07/2024]. See the Terms and Conditions (https://onlinelibrary.wiley.com/terms-and-conditions) on Wiley Online Library for rules of use; OA articles are governed by the applicable Creative Commons License

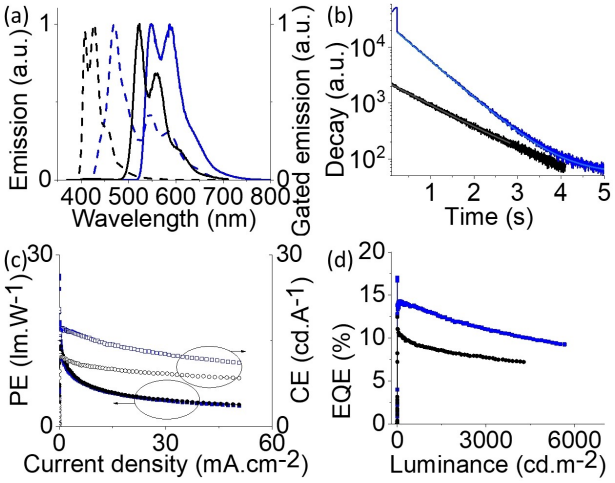

Figure 3. **[4]C-Bu-Cbz** (**9**) in blue and **[4]L-Bu-Cbz** (**10**) in black. (a) Normalized fluorescence (dotted line) and phosphorescence (solid line) spectra at 77 K, in 2-MeTHF. (b) Time-resolved phosphorescence decay. (c) Plot of power efficiency and current efficiency as a function of current density. (d) Roll-off EQE as a function of luminance. Reprinted (adapted) with permission from *Adv. Opt. Mater.* ***2023***, *11*, 2202191. Copyright 2023, Wiley-VCH.

respectively measured at 17 %, 20.6 cd A^{-1} and 25.8 lm W^{-1} (at 0.01 mA cm^2) for **9**. The threshold voltage was also measured low (2.3 V), showing an excellent charges injection. Oppositely, **10** displays, with the same device configuration, significantly lower performance with EQE_{max} of 11.1 %, CE_{max} of 13.0 cd A^{-1} and PE_{max} of 15.7 lm W^{-1} (at 0.07 mA cm^{-2}). Atomic force microscope (AFM) images unveiled a smoother surface for **9** and hence less defect's density compared to **10**, which displays spreading peaks. This is in agreement with the charge carrier mobility (measured by space-charge limited current SCLC in the out-of-plane direction), two times higher for **9** compared to **10** ($\mu^h_{SCLC} = 2.78\times10^{-4}$ $cm^2V^{-1}s^{-1}$ and 1.49×10^{-4} $cm^2V^{-1}s^{-1}$ for **9** and **10** respectively). The reason of the higher performance reached by **9** was not assigned with a complete certitude. However, the authors have proposed different hypotheses such as (i) a better injection of the electrons favoured by a lower LUMO, (ii) a better charge recombination and photon extraction due to a better organization of the nanohoop in thin film, and (iii) a lower lifetime of the triplet state of the nanohoop, which decreases the density of triplet states and the probability of triplet-triplet annihilation. This work, which is the first high performance OLED reported to date, opens a new avenue for the development of nanohoops in PhOLEDs. It should be mentioned that very few data have been published on the phosphorescence and triplet state of nanohoops,[83–87] which is obviously a limiting factor for PhOLED applications. Indeed, the determination of E_T is essential to evaluate the host/guest T_1/T_1 energy transfers.[82] Itami and co-workers have observed, in 2022, that perfluorocyclo-*para*-phenylenes were not fluorescent ($\Phi_F < 0.01$) at room temperature but a bright phosphorescence was observed at low temperature ($\leq$150 K).[87] This behaviour is drastically different to that observed for parents CPPs and show that inter-system crossing occurs much more quickly compared to CPPs. These findings, despite not unravelled yet, are the premises of further materials designs. Indeed, efficient bipolar host materials for PhOLEDs are very often weakly fluorescent.[82,88–90]

In the field of OLED, fluorescent OLEDs[91–93] represent the first generation, phosphorescent OLEDs[89,94–99] the second generation and thermally activated delayed fluorescence (TADF)-based OLED the third one.[100–104] TADF is a photophysical mechanism, in which both singlet and triplet excitons can be harnessed leading to theoretically 100 % internal quantum efficiency through reverse intersystem crossing process.[103,105–107] Although TADF was theoretically predicted for D–A nanohoops by Graham and co-workers in 2017,[108] there is still no report to date of a nanohoop displaying a TADF behaviour. In 2023, Zysman-Colman and co-workers have designed a phenoxazine-decorated [10]CPP-based nanohoop, namely **4PXZPh-[10]CPP** (**11**), and have explored the possibility to use it as TADF emitter in OLEDs (Figure 4).[109] Density functional theory (DFT)-based calculations have shown that HOMO and LUMO of **11** were spatially separated (localized respectively on phenothiazine and CPP moieties). Such spatial separation of HOMO and LUMO density helped to reduce the S_1-T_1 energy gap ΔE_{ST}, that gave rise to a short theoretical ΔE_{ST}. The ultraviolet-visible (UV/Vis) absorption spectra present a maximum at ca 339 and 331 nm for **[10]CPP** and **11** respectively assigned to locally excited (LE) transitions (Figure 4b). For **11**, an additional LE transition centred on the phenyl phenoxazine fragments has been linked to the blue-shifted absorption.

A tail at ca 400 nm was also detected and assigned to a mixed LE state and weak intramolecular charge transfer state (transition from HOMO to LUMO). The emission spectrum of **11** is broad and structureless in the green region ($\lambda^f_{max} = 508$ nm, $\Phi_F = 0.34$), which is in contrast to the slightly vibronically-featured blue emission of **[10]CPP** ($\lambda^f_{max} =$ 470 nm, $\Phi_F = 0.77$). The emission of **11**, which is red-shifted compared to that of **[10]CPP**, was attributed to radiative transition from CT state (characterized by solvatofluorochromism as shown in Figure 4c), whereas LE state was mostly populated in case of **[10]CPP**. Nanohoop **11** in 9-(4-(*tert*-butyl)phenyl)-3,6-bis-(triphenylsilyl)-9*H*-carbazole (CzSi)-doped film (15 wt %) showed strong blue emission with $\lambda^f_{max} = 475$ nm, $\Phi_F = 0.29$, and lifetime $\tau_1 = 4.4$ ns, $\tau_2 =$ 46.3 ns and $\tau_3 = 907.8$ ns. No TADF behaviour was detected. This can be linked to the experimental ΔE_{ST} measurements providing values of 0.50 eV in dichloromethane and 0.68 eV in toluene, significantly larger than the thereotical ΔE_{ST} in gas phase (0.08 eV). A solution-processable fluorescent OLED device was finally architected by integrating **11**: CzSi as an emitting layer in a simple OLED structure (Figure 4d). The device exhibited sky-blue emission with $\lambda^{em}_{max} = 465$ nm, and $EQE_{max} = 1.0$ % at 1.0 mA cm^{-2} (Figure 4e). Despite its low EQE, this work was another contribution on the path of nanohoops in electroluminescent devices.

© 2024 The Authors. Angewandte Chemie International Edition published by Wiley-VCH GmbH

15213773, 0, Downloaded from https://onlinelibrary.wiley.com/doi/10.1002/anie.202402608 by Université De Rennes, Wiley Online Library on [08/07/2024]. See the Terms and Conditions (https://onlinelibrary.wiley.com/terms-and-conditions) on Wiley Online Library for rules of use; OA articles are governed by the applicable Creative Commons License

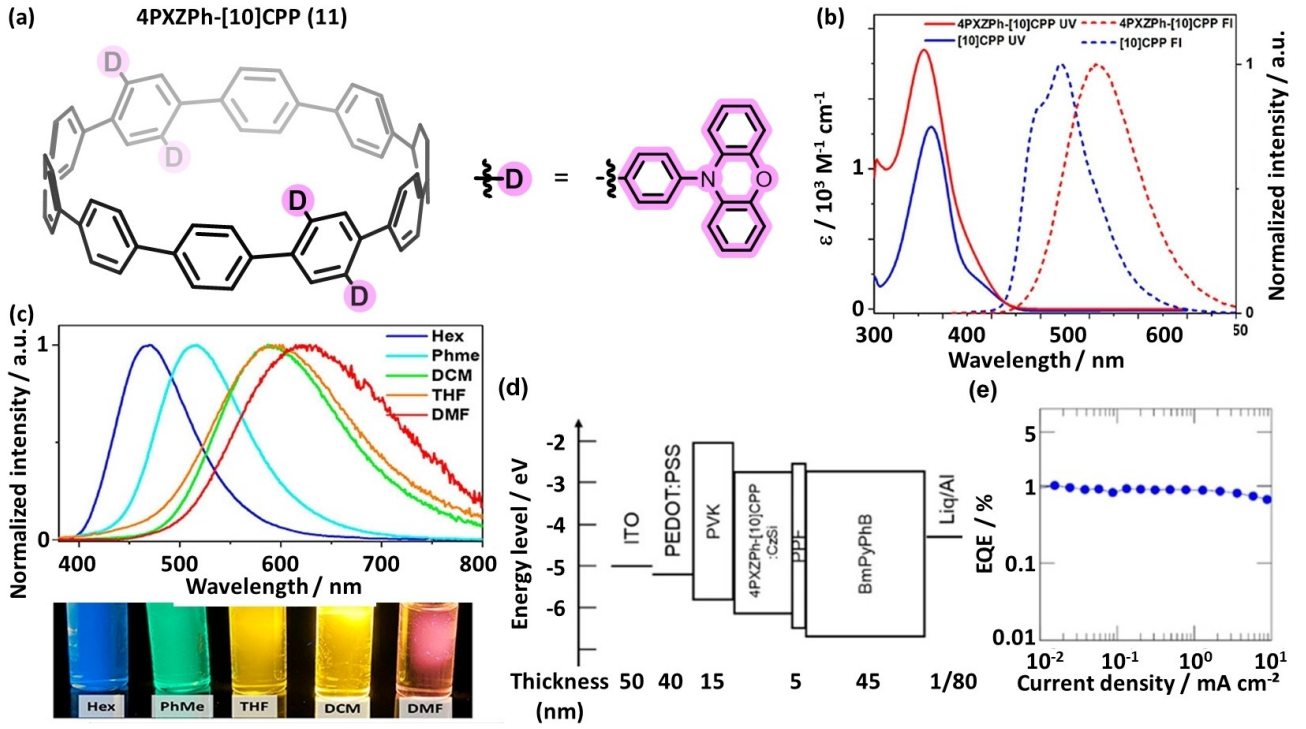

Figure 4. **4PXZPh-[10]CPP (11)**. (a) molecular structure, (b) absorption (solid line) and fluorescence (dotted line) spectra of **11** (in red) and **[10]CPP** (in blue, in toluene), (c) solvent polarity-dependent emission spectra and solution colour images, (d) representation of a **11**:CzSi-constituted OLED device, and (e) EQE vs current density plot. Reprinted (adapted) with permission from *Org. Lett.* **2023**, *25*, 998–1002. Copyright 2023 American Chemical Society.

3.2. Nanohoops as an Active Layer in OPVs

Organic photovoltaics (OPV) is also a very important research area in organic electronic technologies[110–115] and again, nanohoops are almost absent from this key field. In 2016, Nuckolls group introduced π-conjugated macrocycles constituted of perylene diimide chromophore as n-type electronic material in organic photovoltaics.[63] They synthesized two nanohoops, namely **cPBPB** (**12**) and **cP$_4$** (**13**), as well as their acyclic polymer counterparts **a(PB)$_n$** (**14**) and **aP$_n$** (**15**), and compared their photovoltaic efficiency (see structures in Figure 5). The OPV devices were fabricated by association of polymer **PTB7-Th** (structure in Figure 5) as electron donor and cyclic **12** or acyclic **14** as acceptor providing average PCE values of 3.3 % and 1.1 % and short-circuit current density $J_{sc} = 9.2$ mA cm^{-2} and 4.2 mA cm^{-2}, for **12** and **14**, respectively. The comparison of the nanohoop **13** and the polymer **15** gave similar results. The authors remarkably noted that cyclic compounds provide an amplification of PCE values compared to their acyclic counterparts. The best performance obtained for the nanohoops was attributed to the fact that they absorbed in the entire UV/Vis region (300–700 nm), displaying a red-shifted absorption compared to their acyclic polymeric analogues. The HOMO–LUMO gap of nanohoops was hence smaller than that of their corresponding linear analogs (for example, $E_{gap} = 1.79$ eV for **13** and 1.89 eV for **15**). Therefore designing nanohoops gives chemists access to new OSCs displaying narrower band gaps than their linear analogues. Furthermore, to probe the charge transport properties, OFET devices were fabricated with both cyclic and acyclic derivatives, revealing notably higher electron mobility values for the macrocycles ($\mu^e_{FET\_sat} = 1.5\times10^{-3}$ cm^2 V^{-1} s^{-1} for both **12** and **13**, $\mu^e_{FET\_sat} = 2.3\times10^{-4}$ cm^2 V^{-1} s^{-1} for **14** and $\mu^e_{FET\_sat} = 1.9\times10^{-5}$ cm^2 V^{-1} s^{-1} for **15**).

The higher OPV performance obtained for the macrocycles has been ascribed not only to high molar extinction coefficient in the visible region, but also to efficient intermolecular interactions in solid state, higher electron transporting capabilities, better phase separation, and improved surface morphologies. This report has shown how cyclization of linear molecules improved device performance. The same group has also investigated the role of molecular conformations in such D–A conjugated nanohoops in order to improve OPV and organic photodetectors (OPD) performance. They have synthesized oligomeric helical perylene diimide dimers covalently conjugated with bithiophene donors in a *cis* or *trans* geometry (***cis*-cDBDB** (**16**) and ***trans*-cDBDB** (**17**), Figure 6).[116] DFT calculations demonstrated that compound **16** adopted 'tent conformation' with more flexibility. On the contrary, for **17**, it was observed a 'upright conformation' with a higher nanohoop strain ($E_{strain} = 9.5$ kcal/mol and 18.6 kcal/mol for **16** and **17**, respectively), as presented in Figure 6. The different conformations of the two nanohoops affected therefore their photophysical and charge transport properties. The *trans*-isomer **17** possessed sharp vibrational features in both absorption and emission, whereas *cis*-isomer **16** presented

© 2024 The Authors. Angewandte Chemie International Edition published by Wiley-VCH GmbH

15213773, 0, Downloaded from https://onlinelibrary.wiley.com/doi/10.1002/anie.202402608 by Université De Rennes, Wiley Online Library on [08/07/2024]. See the Terms and Conditions (https://onlinelibrary.wiley.com/terms-and-conditions) on Wiley Online Library for rules of use; OA articles are governed by the applicable Creative Commons License

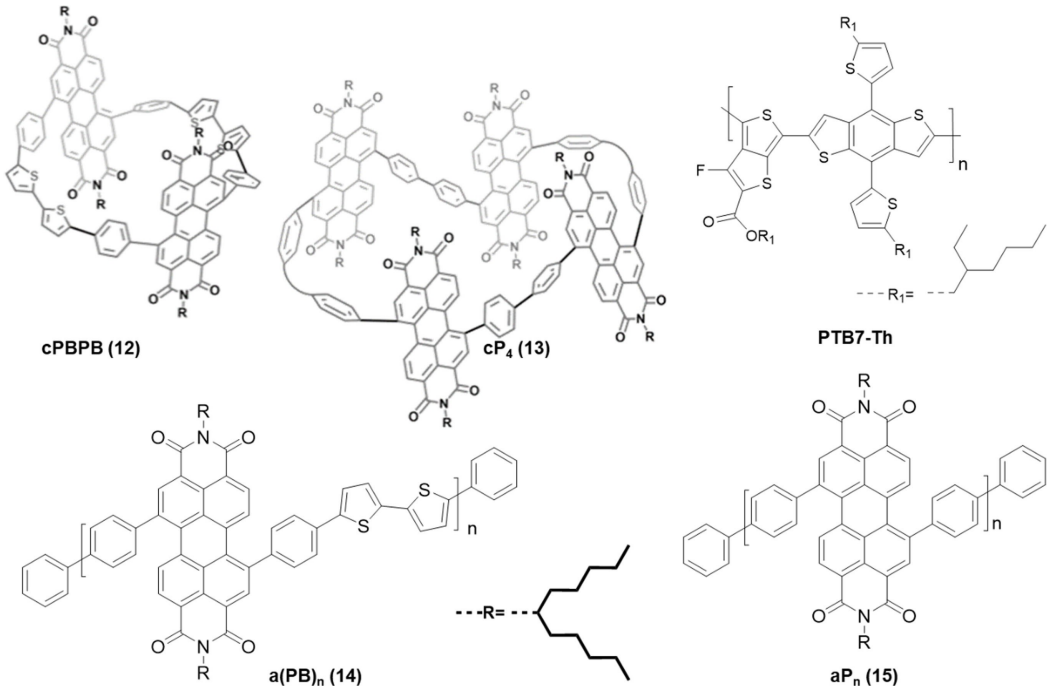

Figure 5. Perylenediimide-constituted nanohoops **cPBPB** (**12**) and **cP$_4$** (**13**) and their corresponding linear polymers **a(PB)$_n$** (**14**) and **aP$_n$** (**15**). Building unit **P** is also presented.

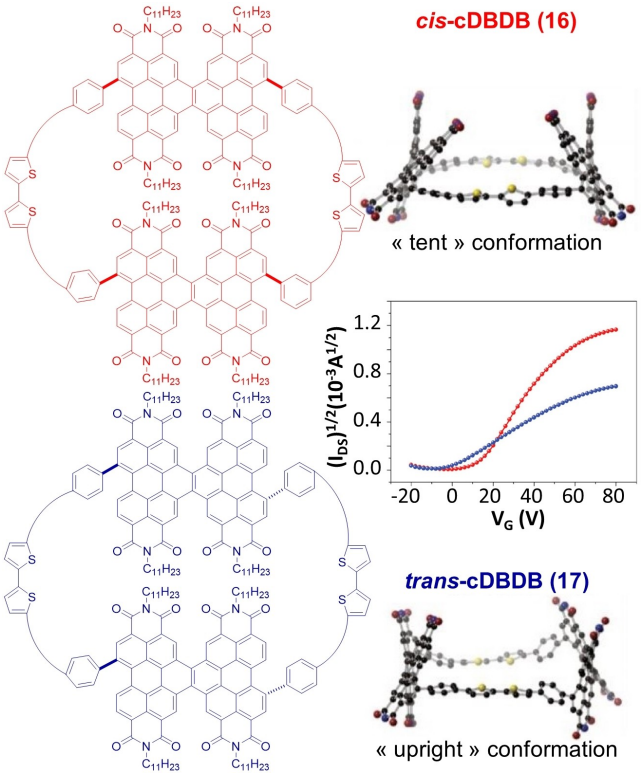

Figure 6. Chemical structures of ***cis*-cDBDB (16)** in red and ***trans*-cDBDB (17)** in blue, their molecular conformations and OFET transfer characteristics. Reprinted (adapted) with permission from *J. Am. Chem. Soc.* **2018**, *140*, 10135–10139. Copyright 2018 American Chemical Society.

broad unstructured spectra. The LUMO energy of both molecules was very close to the LUMO of fullerene derivative **PC$_{61}$BM** ([6,6]phenyl-C61-butyric acid methyl ester), widely used as acceptor in OPV. The field effect (FE) electron mobility values were reported at $\mu^{e}_{FET\_sat} = 4.1\times10^{-3}$ and 1.0×10^{-3} cm^2 V^{-1} s^{-1} for *cis*- (**16**) and *trans*- (**17**) isomers, respectively (Figure 6). Thus, a 4-fold increase was measured for **16** *vs* **17**. The flexible geometry of **16** was assumed to be at the origin of these differences.

Following the concept on the impact of macrocylization on electronic devices performances, the Nuckolls group has investigated OPD devices.[62] One major problem of OPD devices is their high dark current density, which determines their noise current level and sensitivity. This issue is, among other parameters, notably caused by charge defects arising from deformed sp^2 C–C bond and from thermal/photo-activation processes. To overcome the above-mentioned predicaments in OPD devices, nanohoop **13** was investigated (Figures 5 and 7). This nanohoop possesses several beneficial properties, such as a rigid conjugated cyclic architecture resulting in few numbers of charge defects and high electron transport ability. No covalent defects were observed upon photo/thermal activation of the molecule, and more importantly, **13** presented a high molar extinction coefficient in the visible region. In the light of these appealing properties, OPD devices were then constructed with **PTB7-Th** (Figure 5) as donor blended with **13**. The device architecture, which does not include any extra carrier blocking layers usually used in fullerene-based devices, is shown in Figure 7a. This device revealed low dark current density ($J_d = 1.4\times10^{-10}$ A cm^{-2}) at −0.1 V and high photocurrent value ($I_{ON}/I_{OFF} > 10^7$ at −0.1 V), as shown in Figure 7b. A record-

© 2024 The Authors. Angewandte Chemie International Edition published by Wiley-VCH GmbH

15213773, 0, Downloaded from https://onlinelibrary.wiley.com/doi/10.1002/anie.202402608 by Université De Rennes, Wiley Online Library on [08/07/2024]. See the Terms and Conditions (https://onlinelibrary.wiley.com/terms-and-conditions) on Wiley Online Library for rules of use; OA articles are governed by the applicable Creative Commons License

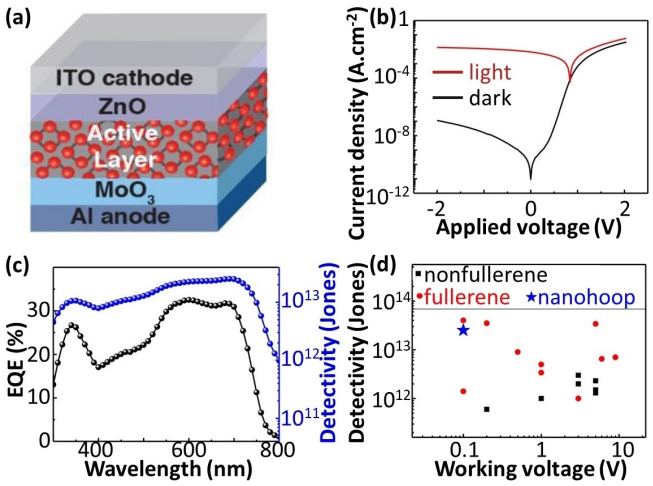

Figure 7. **cP$_4$(13)** (a) Inverted OPD device architecture. (b) Current density *vs* voltage graph under dark and light (simulated air mass 1.5 global irradiation) conditions. (c) EQE and specific detectivity spectra calculated at −0.1 V bias voltage. (d) Plot showing a comparison of the detectivity of three types of OPD devices in a specific range of working voltage. Reprinted (adapted) with permission from *J. Am. Chem. Soc.* **2016**, *138*, 16426–16431. Copyright 2016 American Chemical Society.

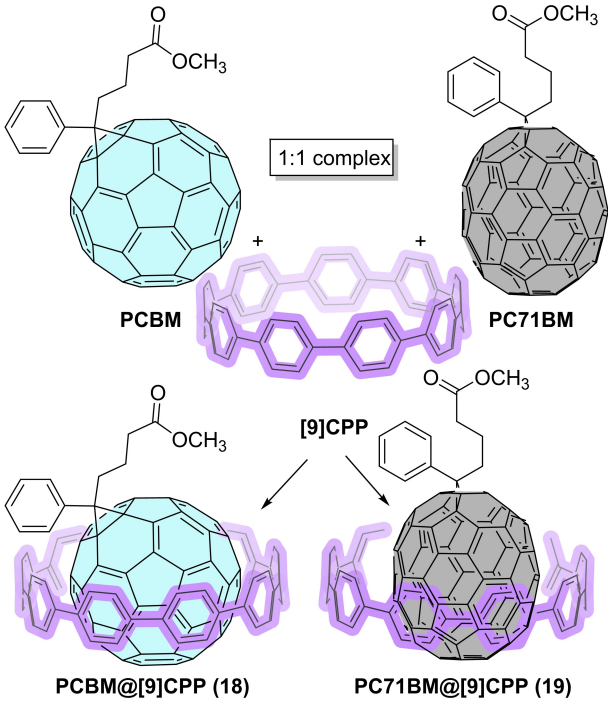

Figure 8. Illustration of **[9]CPP**-fullerene complexation.

breaking detectivity value of ca 10^{14} Jones at near zero bias voltage was achieved (Figure 7c–d). The efficiency of these devices was equivalent to the best fullerene-based OPDs reported at that time (note that fullerene is also a curved molecule). The sensitivity at low working voltages (< 0.1 V) was also a record for non-fullerene OPDs.

To finally analyse the key role played by the cyclic constrained geometry of **13** in OPD devices, the authors comparatively investigated the dark current density with the acyclic counterpart **15** (Figure 5), which endowed relatively higher dark current, $J_d = 1.0\times10^{-9}$ A cm^{-2} at −0.1 V. The OPD sensitivity measured with **15** was lower (4.8×10^{12} Jones) than its cyclic version **13**. The best performance for **13** compared to **15** was ascribed to charge defects caused by terminal groups in linear backbone of **15**.

The unique curved geometry and defined cavity of nanohoops have been a fantastic playground for supramolecular chemists to investigate host–guest complexation.[34,50,117–124] In 2020, Tao and co-workers employed **[9]CPP** as third additive component in the active layers of fullerene-based OPV device, which promoted to form 1:1 **[9]CPP**-fullerene complexes, **PCBM@[9]CPP** (**18**) and **PC$_{71}$BM@[9]CPP** (**19**), thanks to favourable concave-convex π- π interaction (Figure 8).[125] It was observed that addition of **[9]CPP** strikingly enhanced the molar extinction coefficient of the **PC$_{71}$BM@[9]CPP** system in the UV/Visible region, which was an important feature for increasing the PCE value. Initially, the binary device made of **PTB7-Th** (Figure 5) and **PC71BM** at 1:1.5 weight ratio, exhibited fill factor of 65.49 %, V_{oc} of 0.79 V, J_{sc} of 17.9 mA cm^{-2} and PCE value of 9.26 %. Noteworthy, after integration of **[9]CPP** at different weight% ratio, the ternary device having configuration **PTB7-Th:[9]CPP:PC71BM** (in 1:0.1:1.5 ratio) showed amplification of PCE values (10.49 %) as well as other key device data, such as fill factor of 68.13 % and J_{sc} of 19.27 mA cm^{-2}. The improved solar cell efficiency for the ternary system is assigned to an improvement of film surface morphologies. The binary system, made of **PTB7-Th** and **PC$_{71}$BM**, displayed nanofiber arrangement with strong aggregation tendency of fullerene. Interestingly, addition of **[9]CPP** induced greater phase separation by minimizing the aggregation, producing lower sized domain. This phase separation gave rise to effective exciton dissociation and consequently better exciton migration, which was reflected in improvement of carrier mobility. The carrier mobility for binary and ternary devices were measured at $\mu^h = 8.45\times10^{-4}$ cm^2 V^{-1} s^{-1} and $\mu^e = 4.07\times10^{-4}$ cm^2 V^{-1} s^{-1} (binary: **PTB7-Th:PC$_{71}$BM**) and $\mu^h = 1.52\times10^{-3}$ cm^2 V^{-1} s^{-1} and $\mu^e = 1.57\times10^{-3}$ cm^2 V^{-1} s^{-1} (ternary: **PTB7-Th:[9]CPP:PC$_{71}$BM**).

3.3. Charge Transport Studies by OFET Devices and the SCLC Technique

In organic electronics, charge transport is a central concept, which drives the efficiency of the three main devices, namely OLED, OFET and OPV.[126] Studying the charge transport of nanohoops and unravelling how it can be improved is an important part of their development. In 2017, Yamago and co-workers have reported the gram scale preparation of **[10]CPP** and its tetraalkoxy derivatives (**20**–**24**), allowing their employment as electron-transport materials (Figure 9).[127] Introduction of alkoxy chains (butyl, hexyl, octyl, 2-ethyl-1-hexyl) or of benzyloxy unit on the CPP backbone significantly improved the solubility of **[10]CPP**-based

© 2024 The Authors. Angewandte Chemie International Edition published by Wiley-VCH GmbH

15213773, 0, Downloaded from https://onlinelibrary.wiley.com/doi/10.1002/anie.202402608 by Université De Rennes, Wiley Online Library on [08/07/2024]. See the Terms and Conditions (https://onlinelibrary.wiley.com/terms-and-conditions) on Wiley Online Library for rules of use; OA articles are governed by the applicable Creative Commons License

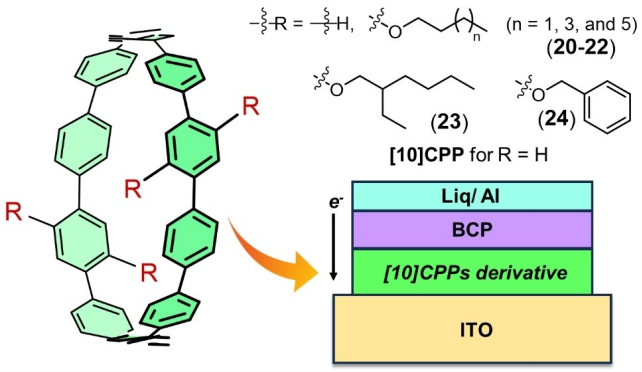

Figure 9. Structural representation of tetraalkoxy-substituted [10]CPPs (**20**–**24**) and the device used.

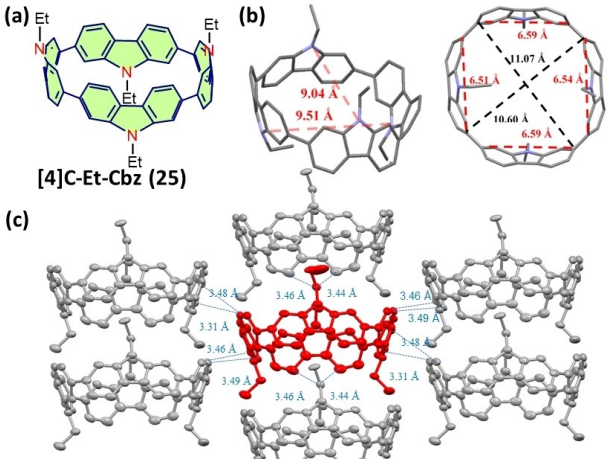

Figure 10. **[4]C-Et-Cbz**: (a) Structural representation, (b) crystal structure, and (c) packing diagram. Reprinted (adapted) with permission from *Chem. Eur. J 2019, 25*, 7740–7748. Copyright 2019 Wiley-VCH.

derivatives in organic solvents (as for example, 28 mmol L^{-1} and 0.38 mmol L^{-1} in $CDCl_3$ at 25 °C for **23** and **[10]CPP** respectively). This characteristic allows to use them in solution-processing devices. In solution, the tetraalkoxy-substituted CPPs displayed absorption maxima at ca 340–345 nm. Noteworthy, they depicted a green emission in solution (maxima at 475–479 nm) with high fluorescence quantum yields (Φ_F = 0.59–0.62). Their photophysical response in thin-film state did not vary from the solution state, showing absorption and emission in similar region, possibly due to weak intermolecular interactions. The ionization potential (measured by an atmospheric photoelectron spectrophotometer) and electron affinity (estimated from the ionization potentials and HOMO–LUMO gaps obtained from the absorption spectra of the film) values were determined as ca. 6.0 and 3.3 eV, respectively, which were close to the values of **PCBM**, signifying their potential as electron accepting materials. Eventually, in this series of CPP derivatives, the spin-coated film of compound **20** exhibited a low electron mobility value μ^e_{SCLC} = 4.5×10^{-6} $cm^2V^{-1}s^{-1}$ in SCLC region, providing a first benchmark CPP derivatives.

Following this work, our group has reported the incorporation of a nanohoop, namely, [4]cyclo-*N*-ethyl-2,7-carbazole (**[4]C-Et-Cbz** (**25**), Figure 10a) in OFET device and has started to deeply study the charge transport properties of cyclocarbazoles.[128] One important feature in this work, and beyond the device applications, was linked to the improvement in term of synthesis. In this work, an interesting yield of 27 % for **25** was reached. Crystal structure shows that the upper portion of carbazole moieties was tilted towards the inner cavity of **25** (Figure 10b). Moreover, carbazoles are also involved in short contacts with either their own pending ethyl chain or with the ethyl chain of a surrounding molecule (3.44 and 3.46 Å), showing that the pending chains have a role in the packing diagram (Figure 10c). This feature could be used to tune the supramolecular arrangement of such nanohoops by alkyl chain engineering. The higher HOMO energy of **25** (−5.17 eV) compared to that of **[8]CPP** (−5.28 eV, Figure 1) has revealed, as expected, the electron rich nature of the [4]-cyclocarbazole. Nitrogen-bridged-nanohoop **25** exhibited an emission centred at 486 nm in cyclohexane, whereas that of **[8]CPP** was red shifted to 528 nm, regardless their absorption in same region.[129] Thus, the introduction of *N*-containing bridges in **[8]CPP** led to a remarkable blue shift of the fluorescence. The most important feature in this work was undoubtedly the OFET incorporation and the resulting first detailed charge transport studies in the field of nanohoops.

Considering that carbazole-based linear structures have been widely used in organic electronics,[79,130–133] studying their nanohoops counterparts appeared relevant to develop new generations of organic materials. p-Type OFET, with a bottom-gate bottom-contact (BG-BC) architecture, using **25** as active layer was then fabricated and characterized. A hole mobility value $\mu^h_{FET\_sat}$ of 1.0×10^{-5} $cm^2V^{-1}s^{-1}$, a threshold voltage V_{TH} of −24 V, and an on-off ratio of the drain current I_{Don}/I_{Doff} = 4.26×10^4 were notably extracted. Despite low performance, this work has revealed that CPP derivatives could be successfully incorporated in OFETs and has opened the door to the rational design of nanohoops as functional materials for electronics.

As above mentioned, since the first example of nanohoops in 2008,[1] the synthetic access has always been the cornerstone of this field and has slowed down its development in materials science and particularly in organic electronics. Following the first OFET studies presented above and to fill the gap between nanohoops and organic electronics by allowing precise charge transport investigations, synthetic optimizations of the Pt approach on [4]-cyclocarbazoles has been investigated by our group in 2021.[129] Thus, a series of [4]-cyclocarbazoles bearing different alkyl chains on the nitrogen atom, ethyl, butyl, and hexyl, **[4]C-Et-Cbz** (**25**), **[4]C-Bu-Cbz** (**9**), and **[4]C-Hex-Cbz** (**26**) respectively were synthesized in very high yields (52–64 %, Figure 11g). This synthetic improvement was highly beneficial for further device optimization. The modification of the substitution on the nitrogen atom was performed in order to tune the supramolecular arrangement

© 2024 The Authors. Angewandte Chemie International Edition published by Wiley-VCH GmbH

15213773, 0, Downloaded from https://onlinelibrary.wiley.com/doi/10.1002/anie.202402608 by Université De Rennes, Wiley Online Library on [08/07/2024]. See the Terms and Conditions (https://onlinelibrary.wiley.com/terms-and-conditions) on Wiley Online Library for rules of use; OA articles are governed by the applicable Creative Commons License

and then the charge transport properties. **[8]CPP**, which also possesses eight phenyl rings, was also investigated in this work in order to check the impact of the presence/absence of the nitrogen bridge on the charge transport properties of the nanohoop. This work was the first detailed structure-properties relationship study of a nanohoop series focusing on their charge transport properties in both SCLC and OFET electronic devices. When an application in electronic devices is envisaged, studying thermal and morphological behaviours are particularly important. The decomposition temperature (Td) determined by thermogravimetric analysis (TGA) and the different phases transition, especially the glass transition and the crystallization temperatures (Tc), determined by differential scanning calorimetry (DSC), are classically measured. Indeed, these data are crucial for the device stability and for the evaporation processes. However, thermal and morphological data were very rarely reported in nanohoops literature. TGA and DSC investigations have revealed high thermal and morphological stability (Td range 335–355 °C) for these [4]-cyclocarbazoles, which made them advantageous for device application. The presence of the different alkyl chains significantly tunes the morphological properties as observed by polarized optical microscopy and DSC. Indeed, the fine crystalline powders of **25** and **26** did not show any phase transition on heating from room temperature onward and up to decomposition. After release of the lattice solvent (ca 170 °C), **9** was also crystalline and displayed an irreversible endothermic crystalline rearrangement (at $T_C = 231$ °C). The new crystalline form was kept on the following heating/cooling run until decomposition. For **[8]CPP**, Td is recorded at 420 °C, and DSC did not reveal any phase transition. Thanks to the absence of alkyl chains in **[8]CPP**, its thermal properties are particularly great. Interestingly, it was also reported that the molecular organization of **[8]CPP** was analogous to that of both **25** and **26**. However, the arrangement of the carbazole nanohoops is constrained by the rejection of the alkyl substituents in the interlayers. Small- and wide-angle X-Ray scattering experiments were also performed and have confirmed the role played by the alkyl chain on the solid-state arrangements in the powder.

In this work, an interesting comparison of the bridge influence was also done. The HOMO levels of **[4]C-diEt-F 27** (displaying four carbon bridges), **25** (displaying four nitrogen bridges) and **[8]CPP** (without bridge) were evaluated at −5.23, −5.17 and −5.28 eV respectively, showing that the presence of the bridge and its nature (C *vs* N) impact the HOMO energy level (see structures in Figure 11g). The increase of the HOMO level from **[8]CPP** to **27** was assigned to the increased degree of conjugation imposed by the bridges, which decrease the average dihedral angle between the connected phenyl rings. The additional upward shift of the HOMO in the tetracarbazole derivatives **9** and **25**–**26** was associated to the higher electron-rich character of the carbazole building unit. The authors also mentioned that this HOMO trend is the same than that of their constituting units: *N*-ethylcarbazole (HOMO = -5.52 eV) displays a higher HOMO than 9,9'-diethylfuorene (HOMO = -5.71 eV) and biphenyl (HOMO = -6.15 eV). This indicated that the HOMO of these three nanohoops were driven by the intrinsic nature of their building units, which was not the case for the position of the main absorption band (Figure 11a). The cathodic explorations have shown that the LUMO levels of [4]-cyclocarbazoles **9** and **25/26** (ca. −2.40 and −2.22/−2.21 eV respectively) were significantly higher than that of **[8]CPP** (−2.60 eV). This was assigned again to the electron-rich character of the carbazole unit. This is different from what is observed in solution as both absorption and emission are similar for the three cyclocarbazoles (Figure 11b,e). In thin solid film, the emission maxima of **25** appeared at 525 nm, significantly shifted compared to that of **26** ($\lambda^f_{max} = 491$ nm), indicating a strong impact of the alkyl chain on the solid state emission characteristics, resulting from the different intermolecular arrangements (Figure 11f). It is well-known that alkyl chain engineering in linear OSCs is an efficient strategy to modulate their solid-state electronic properties but this feature has not been rationally investigated to date with nanohoops. As for the HOMO/LUMO energy levels, presented above, this work has also precisely compared the absorption and emission properties of **[8]CPP** with their bridged analogues (**[4]C-Et-Cbz 25** and **[4]C-diEt-F 27**), showing that the influence of the presence of the bridge, C or N, is significantly less marked in the case of emission *vs* electrochemical properties.

The heart of this work was dealing with the charge transport properties and particularly the huge difference observed between [4]-cyclocarbazoles and the non-bridged analogue **[8]CPP**. The FE mobility of the three [4]-cyclocarbazoles were evaluated at ca 10^{-5} $cm^2 V^{-1} s^{-1}$ (Figure 12a–c) whereas **[8]CPP** did not provide any FE value. The SCLC mobilities measured for the three [4]-cyclocarbazoles (1.37-2.78×10^{-4} $cm^2 V^{-1} s^{-1}$) were also amplified by 3-order relative to **[8]CPP** (1.21×10^{-7} $cm^2 V^{-1} s^{-1}$). It was also shown that other OFET characteristics (threshold voltage, subthreshold swing, activation energy) were also significantly tuned by changing the alkyl chain lengths, translating the huge impact on the semi-conductor organization. AFM studies performed directly on the OFETs have nicely corroborated the electrical measurements (Figure 12a–d), showing the different film surfaces. If both **9** and **25** presented a regular and smooth morphology with low surface roughness (root mean roughness Rq of 0.421 and 0.837 nm respectively), **26** and more significantly **[8]CPP** displayed a high surface roughness (Rq of 1.47 and 3.67 nm respectively). These data were in accordance with the subthreshold swings, threshold voltages and linear *vs* saturated FE mobilities, which all indicate a better organization of the nanohoops in thin film for both **9** and **25** compared to both **26** and **[8]CPP**. The theoretical electronic couplings between the nanohoops in the single-crystal structures as well as the associated thermally induced fluctuations were also investigated to shed light on the origin of this behaviour. This study has shown the importance of molecular and supramolecular parameters which influence the charge transport in nanohoops and have demonstrated how the charge transport can be significantly tuned by the nature of the building unit (carbazole *vs* non-bridged biphenylene).

© 2024 The Authors. Angewandte Chemie International Edition published by Wiley-VCH GmbH

15213773, 0, Downloaded from https://onlinelibrary.wiley.com/doi/10.1002/anie.202402608 by Université De Rennes, Wiley Online Library on [08/07/2024]. See the Terms and Conditions (https://onlinelibrary.wiley.com/terms-and-conditions) on Wiley Online Library for rules of use; OA articles are governed by the applicable Creative Commons License

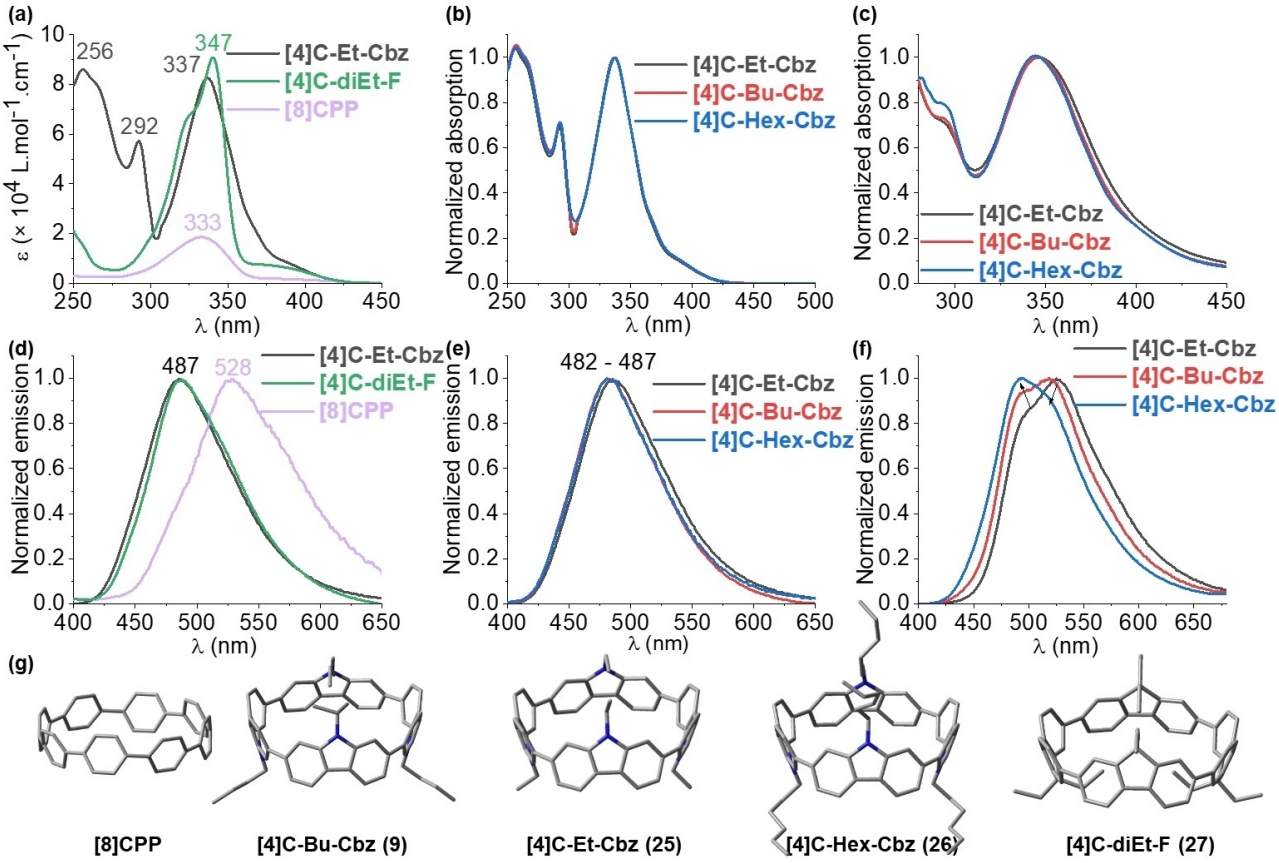

Figure 11. Top: Absorption (a–c) and emission (d–e, excitation wavelength of 340 nm) spectra of **[8]CPP**, **[4]C-Bu-Cbz** (**9**), **[4]C-Et-Cbz** (**25**), **[4]C-Hex-Cbz** (**26**) and **[4]C-diEt-F** (**27**) in cyclohexane (a, b, d and e) and in the solid state (c and f). Bottom: Molecular structures obtained by X-ray crystallography (g). Reprinted (adapted) with permission from *J. Am. Chem. Soc.* **2021**, *143*, 8804–8820. Copyright 2021 American Chemical Society.

Several works exist on the impact of the size on the structural and electronic properties of bridged nanohoops, two key factors for electronic applications.[40,47,75] However, despite the promising mobilities predicted by the theoretical work of Houk and Yavuz and co-workers in 2019 (see above),[30] the role of nanohoop size on their charge transport properties still remained an untold story from the experimental point of view. This encouraged our group to work towards this goal. Thus, in 2023, the effect of nanohoop size on charge mobility in OFET device for two [n]-cyclocarbazoles, namely **[4]C-Bu-Cbz** (**9**) and **[5]C-Bu-Cbz** (**28**) and their non-bridged analogues **[8]CPP** and **[10]CPP**, was reported (Figure 13).[48] Using the optimized protocol discussed in the previous work,[129] the targeted nanohoops were synthesized with a yield of 58 % (**9**) and 2 % (**28**). As already observed for cyclofluorenes,[47] the nanohoop with 5 building units is formed during the synthesis of its analogue with 4 units. This is, from a mechanistic point of view, extremely interesting as this Pt-assisted reaction is far from having revealed all its subtleties. The absorption properties, in solution, of both nanohoops were similar, but the emission maximum of **28** showed a 51 nm blue shift compared to its 4-membered analogue **9**. In terms of emission properties, **28** was a more efficient fluorophore than **9** as evidenced by the quantum yield values ($\Phi_F = 0.56$ and 0.20 for **28** and **9**, respectively). Both the HOMO and LUMO energy levels decreased while increasing the nanohoop size. Interestingly, profound decrease of LUMO gave rise to an overall energy gap contraction for **28** compared to **9**, while the trend is the opposite for their non-bridged analogues: the gap is smaller for **[8]CPP** compared to **[10]CPP**. This difference between these two families of nanohoops is linked to the presence of an odd number of bridges in **28**, which highly decreases its symmetry. Finally, incorporation of both [n]-cyclocarbazoles **9** and **28** and their non-bridged version **[8]CPP** and **[10]CPP** as active layers in OFETs showed no FE mobility for CPPs, whereas cyclocarbazoles exhibited marked response in the device. This result signified a crucial role of bridging N-atoms in amplification of charge transport values for carbazole-based nanohoops. The FE mobility value in saturated regime was measured 4-times higher for [5]-cyclocarbazole **28** than its smaller 4-membered analogue **9** ($\mu^h_{FET\_sat} = 4.22\times10^{-5}$ and 1.04×10^{-5} $cm^2 V^{-1} s^{-1}$ for **28** and **9**, respectively). However, in terms of linear mobility values, [4]-cyclocarbazole **9** possessed relatively greater $\mu^h_{FET\_lin}$ value than its larger analogue **28** ($\mu^h_{FET\_lin} = 1.03\times10^{-5}$ and 0.933×10^{-5} $cm^2 V^{-1} s^{-1}$ for **9** and **28**, respectively). The similar $\mu^h_{FET\_lin}$ and $\mu^h_{FET\_sat}$

© 2024 The Authors. Angewandte Chemie International Edition published by Wiley-VCH GmbH

15213773, 0, Downloaded from https://onlinelibrary.wiley.com/doi/10.1002/anie.202402608 by Université De Rennes, Wiley Online Library on [08/07/2024]. See the Terms and Conditions (https://onlinelibrary.wiley.com/terms-and-conditions) on Wiley Online Library for rules of use; OA articles are governed by the applicable Creative Commons License

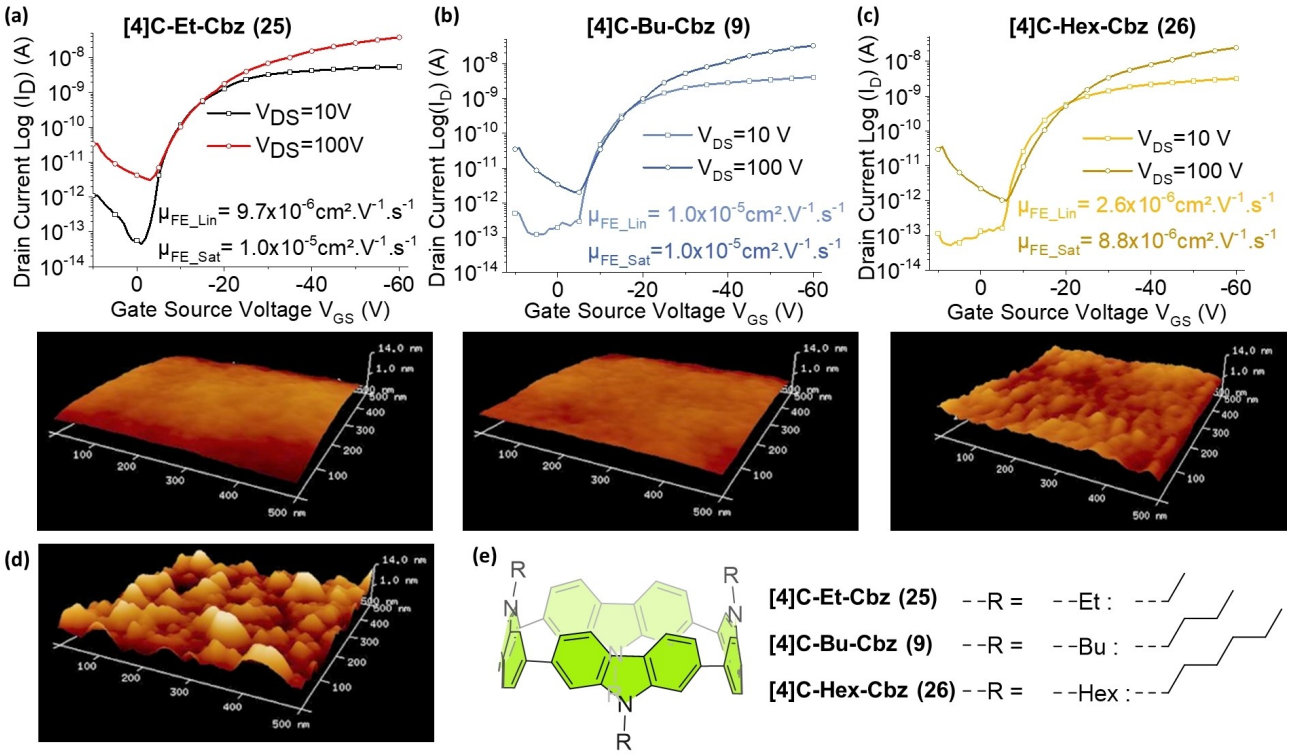

Figure 12. **[4]C-Et-Cbz (25)**, **[4]C-Bu-Cbz (9)**, and **[4]C-Hex-Cbz (26)**. Transfer characteristics in linear and saturated regimes and 2D 500×500 nm^2 AFM images of the semiconducting layer deposited under vacuum on an SU8 insulating layer of the three cyclocarbazoles (a–c) and **[8]CPP** (d) and chemical structures (e). Reprinted (adapted) with permission from *J. Am. Chem. Soc.* **2021**, *143*, 8804–8820. Copyright 2021 American Chemical Society.

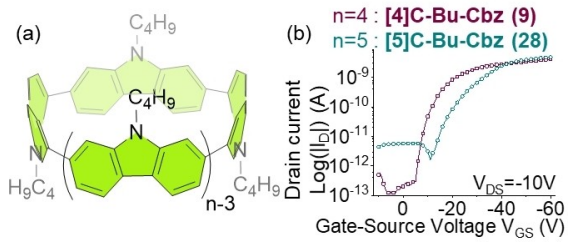

Figure 13. **[4]C-Bu-Cbz** and **[5]C-Bu-Cbz**: (a) Structural representation and (b) transfer characteristics in the linear regime Reprinted (adapted) with permission from *Chem. Eur. J 2023, 29*, e202300934. Copyright 2023 Wiley-VCH.

values obtained for **9** show that the hole mobility in the linear regime is almost unaffected by traps into the OSC. Moreover, other OFET parameters like threshold voltage and subthreshold swing, measured for the two nanohoops, indicated that smaller nanohoops held better molecular arrangement in solid state, whereas the larger showed more structural defects in the thin-film state. It is obvious that the serie investigated in this work does not allow to draw a precise map regarding the size influence and other structure/properties/device performance relationship studies should be performed to go deeper in the precise evolution of the OFET parameters with nanohoop size.

In 2021, Du and co-workers reported a new synthetic strategy to directly functionalize polyaromatic hydrocarbons (PAHs)-based nanohoops by Scholl-reaction following a two-bond approach, in order to achieve large π-extended nanohoops (Figure 14a).[134] The advantage of this strategy was the elimination of strain-influenced side reaction, such as 1,2-phenyl rearrangement shift. Due to its extended π -conjugation, nanohoop **30** demonstrated, in solution, a bathochromic shift in both absorption and emission spectra relative to its precursor **29**. The structured absorption profile of **30** consisted of four vibronic bands at 371, 400, 461, and 491 nm. The emission spectra of **30** was also more structured than that of **29**. Theoretical studies unravelled that the HOMO–LUMO gap of **30** was smaller (2.79 eV) than that of **29** (3.17 eV) due to increasing conjugation. The electron mobility of **30** (~1.8×10^{-4} $cm^2V^{-1}s^{-1}$) was slightly higher than that of **29** (~1.4×10^{-4} $cm^2V^{-1}s^{-1}$), these values being similar to those of [4]-cyclocarbazoles discussed above (Figure 14b). In addition, the authors also brought another example of larger π -extended nanohoop, **[9]CPPH$_{2,11}$** (**31**), constructed on a hexabenzocoronene (HBC) core (Figure 14c).[135] The HBC core is a highly conjugated π-system, which can be considered as a fragment of [12,12] armchair SWCNTs (single-walled CNTs), as shown in Figure 14c. Nanohoop **31** was prepared by Suzuki coupling with a HBC precursor followed by a reductive aromatization reaction. DFT studies have revealed a significant distortion of the HBC unit within the nanohoop and greater strain energy (ca

© 2024 The Authors. Angewandte Chemie International Edition published by Wiley-VCH GmbH

15213773, 0, Downloaded from https://onlinelibrary.wiley.com/doi/10.1002/anie.202402608 by Université De Rennes, Wiley Online Library on [08/07/2024]. See the Terms and Conditions (https://onlinelibrary.wiley.com/terms-and-conditions) on Wiley Online Library for rules of use; OA articles are governed by the applicable Creative Commons License

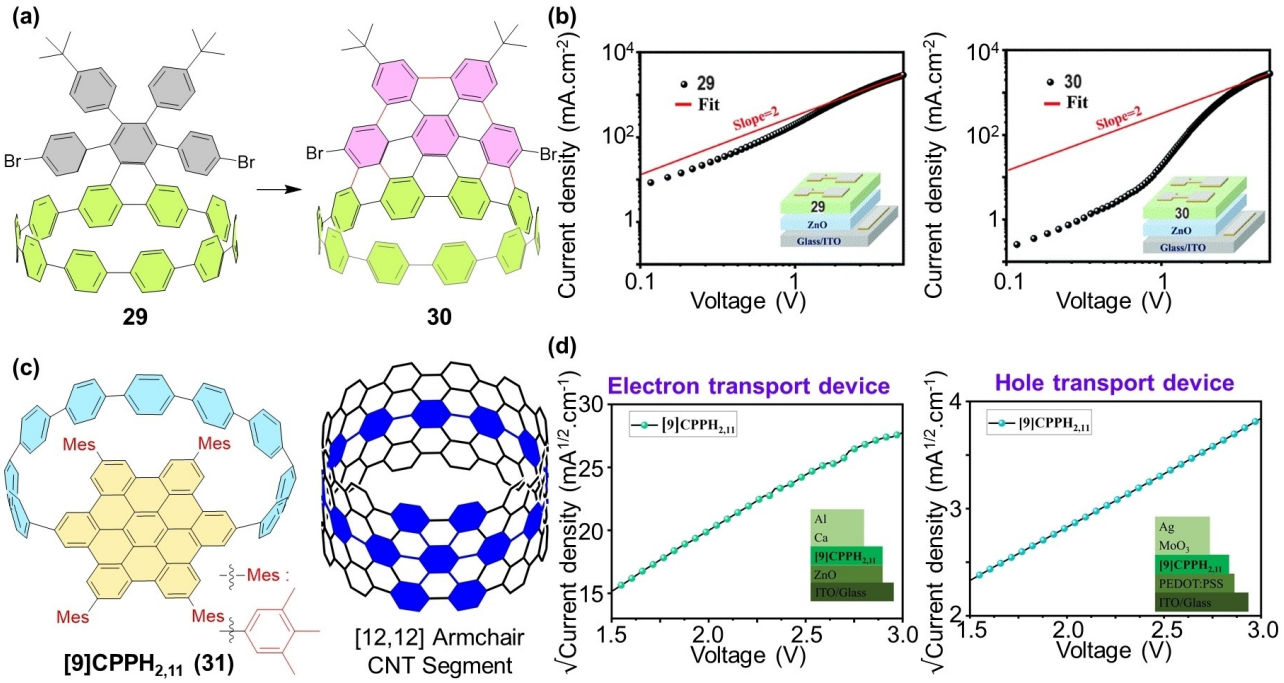

Figure 14. (a) Representation of the longitudinal π-extension of PAH-based nanohoop by a Scholl reaction. (b) Current density vs. voltage graph and the respective fitting curve obtained from the electronic device using compound **29** (left) and compound **30** (right) as an electron transport layer. (c) Structural representation of compound **31**. (d) Current density *vs* voltage graph in the electron and hole transport devices for **31**. Reproduced from Chem. Commun. **2021**, *57*, 9104 with permission from the Royal Society of Chemistry and from *Eur. J. Org. Chem.* **2022**, e202101493; Copyright 2022, John Wiley and Sons.

54 kcal/mol) for **31** than for **[12]CPP** (ca 49 kcal/mol). **31** also exhibited a red shift in absorption and emission compared to **[12]CPP**. Incorporation as electron transporting layer in electron-only device, with architecture ITO/ZnO/**31**/Ca/Al, provides an electron mobility of ~1.82×10^{-4} $cm^2V^{-1}s^{-1}$ (Figure 14d left). Similarly, hole-only device with configuration of ITO/PEDOT:PSS/**31**/MoO_3/Ag was fabricated and provides a hole mobility of ~9.49×10^{-6} $cm^2V^{-1}s^{-1}$ (Figure 14d right). It is interesting to note that electron mobility is higher than hole mobility despite no specific electron-poor functional unit was incorporated in the molecular structure. This feature may deserve attention in the future.

In 2021, Zhu and co-workers have determined the size-dependent charge transport properties for a series of **[n]CPPs** ($n=5$–12) in single molecule device using the scanning tunnelling microscope-break junction (STM-BJ) technique.[136] In single-**[n]CPP** junction, the phenyl rings of CPPs easily and directly interacted with Au electrodes without requirement of any heteroatom containing anchor groups (Figure 15a). This was ascribed to an effective orbital overlap between radially-oriented π-orbitals of phenyl rings and outer orbitals (6 s and 5d) of Au. The highest electrical conductivity was achieved for **[5]CPP** and the conductivity gradually dropped with enlargement of the size of CPPs. The 1D-conductance histogram shown in Figure 15b revealed that the conductance profile became broad for large CPPs, which is possibly due to the overlapping of different conductance peaks as a result of having manifold phenyl

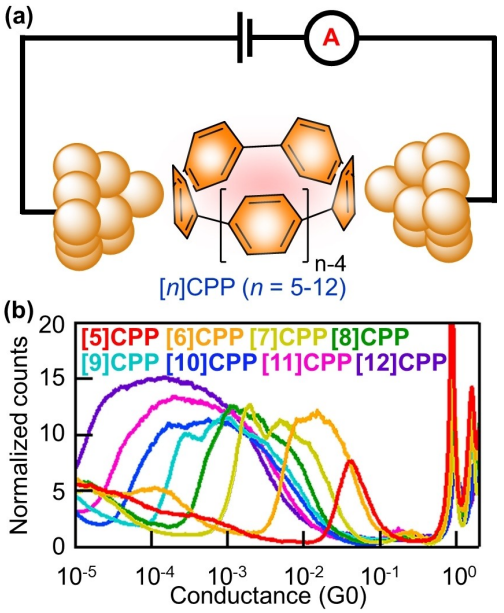

Figure 15. (a) Representation of an **[n]CPP**-based single-molecule junction; orange-coloured spheres represent Au electrodes. (b) 1D-histogram plot showing the conductance for a series of **[n]CPPs** recorded at 100 mV bias voltage. Reprinted (adapted) with permission from *Sci. Adv.* **2021**, *7*, eabk3095; Copyright 2021, American Association for the Advancement of Science.

© 2024 The Authors. Angewandte Chemie International Edition published by Wiley-VCH GmbH

15213773, 0, Downloaded from https://onlinelibrary.wiley.com/doi/10.1002/anie.202402608 by Université De Rennes, Wiley Online Library on [08/07/2024]. See the Terms and Conditions (https://onlinelibrary.wiley.com/terms-and-conditions) on Wiley Online Library for rules of use; OA articles are governed by the applicable Creative Commons License

units interacting with the Au electrodes. On the opposite side, these large CPPs featured high tunnelling attenuation coefficient β (~7.4/nm), which is close to that of saturated alkane analogues (β = 8.3/nm) and higher than that of their linear oligophenyl counterparts (β = 4/nm). Furthermore, theoretical investigations disclosed the greater binding energy of phenyl-Au binding site for smaller nanohoops, the energy being reduced for the larger nanohoops because of less curvature strain as size increased.

The key reasons behind the high conductance of the small CPPs were assigned to the weak torsion angles between phenyl units due to curvature strain. In conclusion, compared to their linear analogues the CPP series studied in this work simultaneously possesses much higher conductance at a relative short transport length and a larger tunneling attenuation coefficient β similar to saturated alkanes. The best performance of the nanohoops compared to their linear analogues has been attributed to the ring strain-induced distortions of π-orbitals.

Following this work, in 2022, Chen, Zhang and co-workers investigated the charge transport properties of a specific family of nanohoops, called nanobelts, using the same STM-BJ technique (Figure 16).[137] They showed that **(6,6)CNB (32)**, consisting of fully fused phenylenes, and its non-bridged analogue **[6]CPP** display lower conductance than the pentagon-embedded nanobelts **[6]CNB_M6 (33)** and **[6]CNB_N3 (34)**, fused by methylene or nitrogen groups respectively, with conductance close to 10^{-1} G_0 (G_0 is conductance quantum), Figure 16. It has been attributed to the greater deformation of **[6]CNB_M6 (33)** and **[6]CNB_N3 (34)** due to their high ring strain induced by the embedding of pentagon units. These results show again that nanohoops are promising for electronics and will motivate the future design of optoelectronic materials using the control of structural distortion of curved π-conjugated systems as a tool to tune the charge transport properties.

In early 2024, a further step was taken with the synthesis and the study of two [4]-cyclocarbazoles incorporating electron-withdrawing units (pyridine or pyrimidine) grafted on the nitrogen atom, namely **[4]C-Py-Cbz** (**35**) and **[4]C-Pm-Cbz** (**36**), as shown in Figure 17.[138] As detailed along this review, the first applications of nanohoops in organic electronics have appeared promising and the next step was to go deeper in their rational design in order to reach high efficiency organic materials. To do so, systematic investigations of the incorporation of electron-rich and/or electron-poor functional units on nanohoops have to be done. Through a structure-properties relationship study, it was shown, in this work, that the electron-withdrawing heterocycle, either pyridine or pyrimidine, when grafted on the nanohoop bridge has an influence on some electronic properties (HOMO/LUMO levels) while others are kept unchanged (fluorescence), see Table 2. In addition, the heterocycle modifies the structural characteristics of the nanohoops and particularly the crystal packing, which in turn modifies the charge transport. Incorporation in electronic devices has revealed that the most electrically efficient OFETs were obtained with **[4]C-Py-Cbz** (**35**)

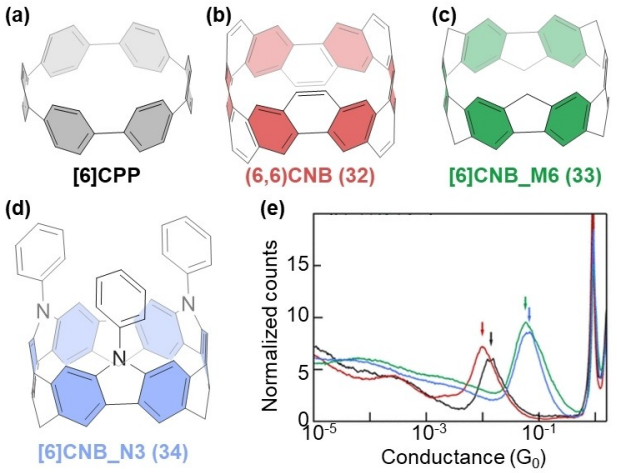

Figure 16. Chemical structures of (a) **[6]CPP**, (b) **(6,6)CNB (32)**, (c) **[6]CNB_M6 (33)** and (d) **[6]CNB_N3 (34)**; e) One-dimensional conductance histograms measured under an applied tip bias voltage of 0.1 V. Reprinted (adapted) with permission from *Sci. Adv.* **2022**, *7*, eade4692; Copyright 2021, American Association for the Advancement of Science.

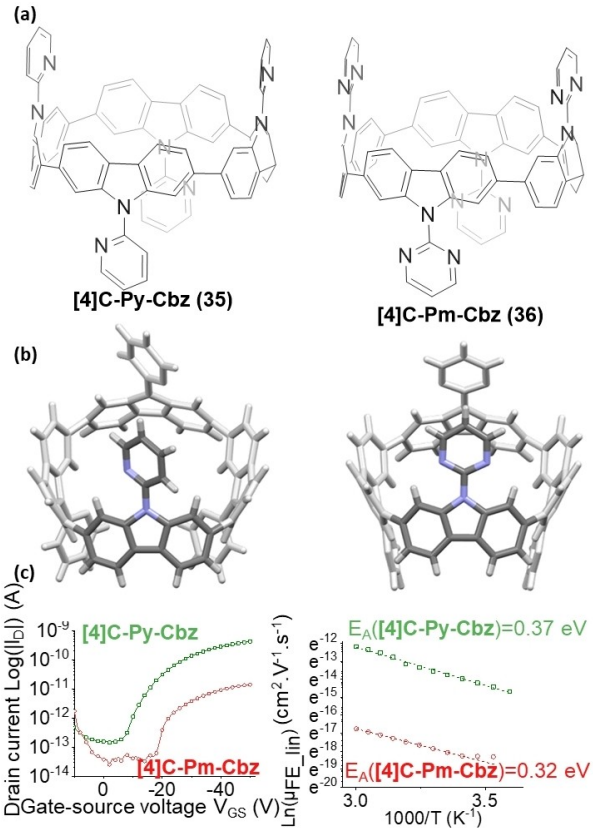

Figure 17. **[4]C-Py-Cbz (35)** in green and **[4]C-Pm-Cbz (36)** in red. (a) Chemical structures, (b) X-ray structures, and (c) transfer characteristics (left) and linear field-effect mobility activation energy (right). Reprinted (adapted) with permission from *Adv. Sci.* **2024**, 2309115. Copyright 2024 Wiley-VCH.

© 2024 The Authors. Angewandte Chemie International Edition published by Wiley-VCH GmbH

15213773, 0, Downloaded from https://onlinelibrary.wiley.com/doi/10.1002/anie.202402608 by Université De Rennes, Wiley Online Library on [08/07/2024]. See the Terms and Conditions (https://onlinelibrary.wiley.com/terms-and-conditions) on Wiley Online Library for rules of use; OA articles are governed by the applicable Creative Commons License

($\mu^{h}_{FET\_lin} = 7\times10^{-7}$ cm^2 V^{-1} s^{-1}/$\mu^{h}_{FET_sat} = 3.4\times10^{-6}$ cm^{2}V^{-1} s^{-1}) although it did not possess the best-organized layer. Indeed, if the linear and saturated mobilities were different for **[4]C-Py-Cbz (35)**, the mobilities of **[4]C-Pm-Cbz (36)** were measured at similar values ($\mu^{h}_{FET_lin} = 1.2\times10^{-8}$ cm^2 V^{-1} s^{-1}/ $\mu^{h}_{FET\_sat} = 2.5\times10^{-8}$ cm^{2}V^{-1} s^{-1}). The electronic couplings between the nanohoops determined at the DFT level have indicated a fundamental origin in these differences of charge transport properties: **[4]C-Py-Cbz (35)** has the advantage of a more 2D-like transport character than **[4]C-Pm-Cbz (36)**, which alleviates the impact of defects and structural organization.[138]

4. Conclusions and Outlook

In the present work, are highlighted the first examples of nanohoops incorporated in organic electronic devices. Organic electronics is, by nature, multidisciplinary and its impressive development in the last twenty years has led to an always growing demand of high-efficiency π-conjugated molecular systems fitting with the specificity of the devices.[39] Developing new molecular architectures such as nanohoops appears, in this context, highly relevant. In organic electronics, the significant development of high efficiency π-conjugated systems perfectly fitting the necessary requirements of a specified device was made possible thanks to the efforts of organic chemists involved in this field. This strategy called *molecular engineering* is one of the pillars of organic electronics but has not been developed with nanohoops yet. The role of physico-chemists and physicists has also been crucial in the development of organic electronic technologies to improve the efficiency of the device itself. This *device engineering* strategy requires numerous optimizations phases, which have only very recently, started to be investigated with nanohoops.[66] The behaviour of nanohoops in term of stability and efficiency is also almost unknown. The first data appear promising. Thus, a new era is currently approaching for nanohoops in electronics and the complementary between chemists and physicists will be the cornerstone of this research field. The chemistry and physics of nanohoops in organic electronics are at their very preliminary stages due to the real synthetic challenges these macrocycles have faced. However, the significant synthetic improvements obtained in recent years, such as the continuous-flow synthesis of CPP building blocks,[139] or the use of Au complexes,[140] now allow to really considering material science as a possible application for nanohoops.

The time has now come to capitalize on these first data. Despite high performance devices (PhOLED and OPD) have already been obtained with nanohoops, these examples remain very rare and the rational design of nanohoops to reach high efficiency organic materials with specific properties is the next important step. The future challenges deal therefore with the design and the synthesis of (i) nanohoops with TADF properties (or Multi-Resonance TADF properties), which can be used in OLEDs, (ii) nanohoops with a high E_T, which can be used as host material in blue PhOLEDs, (iii) nanohoops with a very low LUMO energy level and a high electron mobility for stable n-type OFETs, (iv) nanohoops with a balance mobility ratio of hole and electron for ambipolar OFETs or single-layer PhOLEDs. This list is, obviously, far to be exhaustive but shows exciting directions for the future. Thus, finding relevant design tactics for decreasing the ΔE_{ST}, increasing the E_T or improving the charge carrier mobilities are then the next stage of their evolution. Grafting electron-rich and/or electron-poor molecular fragments either in the backbone of the nanohoop or at its periphery appears as a basic molecular technique to reach above mentioned properties. This strategy has been, for the last 30 years, one of the pillars of the development of linear OSCs. However, as such Donor-Acceptor nanohoops are not significantly developed yet,[138,141] it is difficult to predict their electronic properties and particularly the strength of intramolecular charge transfer. For example, in 2020, Jasti and co-workers have reported, in a theoretical work, the impact of both the curvature and of the spatial position of donor and acceptor groups in CPPs on fluorescence properties. They have shown the strength of the strain to push the limits of low band gap materials.[142] The size of nanohoops and the resulting flexibility could also be considered as a tool for tuning the electronic properties.

The thousands of linear π-conjugated systems, developed for organic electronics in the last 30 years, should thus constitute a formidable library for the development of nanohoop-based materials. Thus, other molecular fragments and/or functional units should be incorporated in the nanohoop backbone in order to rationalize their electronic and physical properties. One can cite, for example, the recent works on functional fluorenone and (9H-fluoren-9-ylidene)malononitrile CPPs,[143–144] which have highlighted the strong impact of these electron-withdrawing units on the CPPs properties. As malonitrile is widely known in n-type OFETs due to its excellent electron accepting capability,[145–148] this opens new applications for functional nanohoops. Considering the huge number of electron-rich and electron-poor functional units developed to date in organic electronics, the possibilities of functionalization appear then unlimited.

Finally, morphological and thermal properties are also key properties in organic electronics but they have been scarcely approached in nanohoops. This part will deserve a deep analysis in the future.

To conclude, the emergence of nanohoops in electronic devices has opened new avenues in the field of organic electronics and gives new applications for these fascinating curved structures. The recent incorporation of nanohoops in organic batteries is also a new very promising application.[149–150] Defining design guidelines of nanohoops will be the first next step to reach the specific properties. This will be the key to reach very high efficiency devices. Thanks to these rational designs, the accurate comparison between linear and curved organic materials could be done. This will allow highlighting the specificities of curved materials and will drive their future molecular design.

© 2024 The Authors. Angewandte Chemie International Edition published by Wiley-VCH GmbH

15213773, 0, Downloaded from https://onlinelibrary.wiley.com/doi/10.1002/anie.202402608 by Université De Rennes, Wiley Online Library on [08/07/2024]. See the Terms and Conditions (https://onlinelibrary.wiley.com/terms-and-conditions) on Wiley Online Library for rules of use; OA articles are governed by the applicable Creative Commons License

Acknowledgements

The authors would like to thank all the researchers in the group involved in the *Nanohoops* project since 2016, Dr L. Sicard, Dr F. Lucas, D. Ari, K. Letellier, E. Dureau. CP and CQ would like to warmly thank Dr Joelle Rault-Berthelot, retired in 2023, who has significantly contributed to this field. We also thank Cefripa (Raman..Charpak Fellowship Program) for PhD and travel grant (RR), the ADEME (Ecoelec Project) and the ANR (N° N°19-CE05-0024-*SpiroQuest* Project) for a PhD grant (CB). CP and EJ thank the University of Rennes for the allocation of a Défi Scientifique 2023-Recherche transdisciplinaire interpoles. CQ thanks Rennes Métropole for the allocation of an AIS grant and the University of Rennes for the allocation of a Défi Scientifique (2024). Dr J. F. Bergamini is thanked for the graphical abstract.

Conflict of Interest

The authors declare no conflict of interest.

Data Availability Statement

As it is a review, there is no data to share

Keywords: Cycloparaphenylenes · Nanohoops · Organic light-emitting diodes · Charge transport · Organic electronics

[1] R. Jasti, J. Bhattacharjee, J. B. Neaton, C. R. Bertozzi, *J. Am. Chem. Soc.* **2008**, *130*, 17646–17647.
[2] H. Takaba, H. Omachi, Y. Yamamoto, J. Bouffard, K. Itami, *Angew. Chem. Int. Ed.* **2009**, *48*, 6112–6116.
[3] S. Yamago, Y. Watanabe, T. Iwamoto, *Angew. Chem. Int. Ed.* **2010**, *49*, 757–759.
[4] J. M. Van Raden, E. J. Leonhardt, L. N. Zakharov, A. Perez-Guardiola, A. J. Perez-Jimenez, C. R. Marshall, C. K. Brozek, J. C. Sancho-Garcia, R. Jasti, *J. Org. Chem.* **2020**, *85*, 129–141.
[5] J. Wang, X. Zhang, H. Jia, S. Wang, P. Du, *Acc. Chem. Res.* **2021**, *54*, 4178–4190.
[6] R. Jasti, C. R. Bertozzi, *Chem. Phys. Lett.* **2010**, *494*, 1–7.
[7] H. Omachi, S. Matsuura, Y. Segawa, K. Itami, *Angew. Chem. Int. Ed.* **2010**, *49*, 10202–10205.
[8] U. H. F. Bunz, S. Menning, N. Martín, *Angew. Chem. Int. Ed.* **2012**, *51*, 7094–7101.
[9] T. Nishiuchi, X. Feng, V. Enkelmann, M. Wagner, K. Müllen, *Chem. Eur. J.* **2012**, *18*, 16621–16625.
[10] H. Omachi, T. Nakayama, E. Takahashi, Y. Segawa, K. Itami, *Nat. Chem.* **2013**, *5*, 572–576.
[11] V. C. Parekh, P. C. Guha, *J. Indian Chem. Soc.* **1934**, *11*, 95.
[12] R. Friederich, M. Nieger, F. Vögtle, *Chem. Ber.* **1993**, *126*, 1723–1732.
[13] S. Hitosugi, W. Nakanishi, T. Yamasaki, H. Isobe, *Nat. Commun.* **2011**, *2*, 492.
[14] M. C. O'Sullivan, J. K. Sprafke, D. V. Kondratuk, C. Rinfray, T. D. W. Claridge, A. Saywell, M. O. Blunt, J. N. O'Shea, P. H. Beton, M. Malfois, H. L. Anderson, *Nature* **2011**, *469*, 72.
[15] C. Huang, Y. Huang, N. G. Akhmedov, B. V. Popp, J. L. Petersen, K. K. Wang, *Org. Lett.* **2014**, *16*, 2672–2675.
[16] A. F. Tran-Van, E. Huxol, J. M. Basler, M. Neuburger, J. J. Adjizian, C. P. Ewels, H. A. Wegner, *Org. Lett.* **2014**, *16*, 1594–1597.
[17] M. Ball, B. Fowler, P. Li, L. A. Joyce, F. Li, T. Liu, D. Paley, Y. Zhong, H. Li, S. Xiao, F. Ng, M. L. Steigerwald, C. Nuckolls, *J. Am. Chem. Soc.* **2015**, *137*, 9982–9987.
[18] D. Myśliwiec, M. Kondratowicz, T. Lis, P. J. Chmielewski, M. Stępień, *J. Am. Chem. Soc.* **2015**, *137*, 1643–1649.
[19] D. Lu, H. Wu, Y. Dai, H. Shi, X. Shao, S. Yang, J. Yang, P. Du, *Chem. Commun.* **2016**, 7164–7167.
[20] Z.-A. Huang, C. Chen, X.-D. Yang, X.-B. Fan, W. Zhou, C.-H. Tung, L.-Z. Wu, H. Cong, *J. Am. Chem. Soc.* **2016**, *138*, 11144–11147.
[21] M. Moral, A. Pérez-Guardiola, E. San-Fabián, A. J. Pérez-Jiménez, J. C. Sancho-García, *J. Phys. Chem. C* **2016**, *120*, 22069–22078.
[22] Y.-Y. Liu, J.-Y. Lin, Y.-F. Bo, L.-H. Xie, M.-D. Yi, X.-W. Zhang, H.-M. Zhang, T.-P. Loh, W. Huang, *Org. Lett.* **2016**, *18*, 172–175.
[23] L. Sicard, O. Jeannin, J. Rault-Berthelot, C. Quinton, C. Poriel, *ChemPlusChem* **2018**, *83*, 874–880.
[24] Y. Xu, R. Kaur, B. Wang, M. B. Minameyer, S. Gsänger, B. Meyer, T. Drewello, D. M. Guldi, M. von Delius, *J. Am. Chem. Soc.* **2018**, *140*, 13413–13420.
[25] D. Wassy, M. Pfeifer, B. Esser, *J. Org. Chem.* **2020**, *85*, 34–43.
[26] K. Li, Z. Xu, J. Xu, T. Weng, X. Chen, S. Sato, J. Wu, Z. Sun, *J. Am. Chem. Soc.* **2021**, *143*, 20419–20430.
[27] A. J. Stasyuk, O. A. Stasyuk, M. Sola, A. A. Voityuk, *Chem. Commun.* **2019**, *55*, 11195–11198.
[28] N. Grabicki, K. T. D. Nguyen, S. Weidner, O. Dumele, *Angew. Chem. Int. Ed.* **2021**, *60*, 14909–14914.
[29] Y. Yang, O. Blacque, S. Sato, M. Juricek, *Angew. Chem. Int. Ed. Engl.* **2021**, *60*, 13529–13535.
[30] J. B. Lin, E. R. Darzi, R. Jasti, I. Yavuz, K. N. Houk, *J. Am. Chem. Soc.* **2019**, *141*, 952–960.
[31] D. Wu, W. Cheng, X. Ban, J. Xia, *Asian J. Org. Chem.* **2018**, *7*, 2161–2181.
[32] M. Ball, B. Zhang, Y. Zhong, B. Fowler, S. Xiao, F. Ng, M. Steigerwald, C. Nuckolls, *Acc. Chem. Res.* **2019**, *52*, 1068–1078.
[33] W.-S. Wong, M. Stępień, *Trends Chem.* **2022**, *4*, 573–576.
[34] Y. Xu, M. von Delius, *Angew. Chem. Int. Ed.* **2020**, *59*, 559–573.
[35] R. Zhang, D. Y. An, J. Y. Zhu, X. F. Lu, Y. Q. Liu, *Adv. Funct. Mater.* **2023**, *4*, 2305249.
[36] A. Stoddart, *Nat. Synth.* **2023**, *2*, 803–804.
[37] E. J. Leonhardt, R. Jasti, *Nat. Chem. Rev.* **2019**, *3*, 672–686.
[38] J.-L. Brédas, S. R. Marder, *The WSPC Reference on Organic Electronics: Organic Semiconductors* **2016**.
[39] Z.-Q. Jiang, C. Poriel, N. Leclerc, *Mater. Chem. Front.* **2020**, *4*, 2497–2498.
[40] F. Lucas, J. Rault-Berthelot, C. Quinton, C. Poriel, *J. Mater. Chem. C* **2022**, *10*, 14000–14009.
[41] T. Iwamoto, Y. Watanabe, Y. Sakamoto, T. Suzuki, S. Yamago, *J. Am. Chem. Soc.* **2011**, *133*, 8354–8361.
[42] E. R. Darzi, R. Jasti, *Chem. Soc. Rev.* **2015**, *44*, 6401–6410.
[43] Y. Segawa, A. Fukazawa, S. Matsuura, H. Omachi, S. Yamaguchi, S. Irle, K. Itami, *Org. Biomol. Chem.* **2012**, *10*, 5979–5984.
[44] M. Fujitsuka, D. W. Cho, T. Iwamoto, S. Yamago, T. Majima, *Phys. Chem. Chem. Phys.* **2012**, *14*, 14585–14588.
[45] K. Okada, A. Yagi, Y. Segawa, K. Itami, *Chem. Sci.* **2017**, *8*, 661–667.
[46] M. Fujitsuka, C. Lu, B. Zhuang, E. Kayahara, S. Yamago, T. Majima, *J. Phys. Chem. A* **2019**, *123*, 4737–4742.

© 2024 The Authors. Angewandte Chemie International Edition published by Wiley-VCH GmbH

15213773, 0, Downloaded from https://onlinelibrary.wiley.com/doi/10.1002/anie.202402608 by Université De Rennes, Wiley Online Library on [08/07/2024]. See the Terms and Conditions (https://onlinelibrary.wiley.com/terms-and-conditions) on Wiley Online Library for rules of use; OA articles are governed by the applicable Creative Commons License

[47] L. Sicard, F. Lucas, O. Jeannin, P. A. Bouit, J. Rault-Berthelot, C. Quinton, C. Poriel, *Angew. Chem. Int. Ed.* **2020**, *59*, 11066–11072.
[48] F. Lucas, C. Brouillac, N. McIntosh, S. Giannini, J. Rault-Berthelot, C. Lebreton, D. Beljonne, J. Cornil, E. Jacques, C. Quinton, C. Poriel, *Chem. Eur. J.* **2023**, *48*, e202300934.
[49] C. Camacho, T. A. Niehaus, K. Itami, S. Irle, *Chem. Sci.* **2013**, *4*, 187–195.
[50] Z. Zhou, Z. Wei, T. A. Schaub, R. Jasti, M. A. Petrukhina, *Chem. Sci.* **2020**, *11*, 9395–9401.
[51] J. S. Wossner, D. Wassy, A. Weber, M. Bovenkerk, M. Hermann, M. Schmidt, B. Esser, *J. Am. Chem. Soc.* **2021**, *143*, 12244–12252.
[52] G. Povie, Y. Segawa, T. Nishihara, Y. Miyauchi, K. Itami, *J. Am. Chem. Soc.* **2018**, *140*, 10054–10059.
[53] Y. Xu, F. Steudel, M. Y. Leung, B. Xia, M. von Delius, V. W. W. Yam, *Angew. Chem. Int. Ed. Engl.* **2023**, *52*, e202302978.
[54] E. Kayahara, V. K. Patel, S. Yamago, *J. Am. Chem. Soc.* **2014**, *136*, 2284–2287.
[55] L. Adamska, I. Nayyar, H. Chen, A. K. Swan, N. Oldani, S. Fernandez-Alberti, M. R. Golder, R. Jasti, S. K. Doorn, S. Tretiak, *Nano Lett.* **2014**, *14*, 6539–6546.
[56] M. Banerjee, R. Shukla, R. Rathore, *J. Am. Chem. Soc.* **2009**, *131*, 1780–1786.
[57] H. Jia, Y. Gao, Q. Huang, S. Cui, P. Du, *Chem. Commun.* **2018**, *54*, 988–991.
[58] H. Omachi, Y. Segawa, K. Itami, *Acc. Chem. Res.* **2012**, *45*, 1378–1389.
[59] L. Zhang, G. Zhang, H. Qu, Y. Todarwal, Y. Wang, P. Norman, M. Linares, M. Surin, H. J. Zhang, J. Lin, Y. B. Jiang, *Angew. Chem. Int. Ed. Engl.* **2021**, *60*, 24543–24548.
[60] Y. Li, A. Yagi, K. Itami, *J. Am. Chem. Soc.* **2020**, *142*, 3246–3253.
[61] T. C. Lovell, S. G. Bolton, J. P. Kenison, J. Shangguan, C. E. Otteson, F. Civitci, X. Nan, M. D. Pluth, R. Jasti, *ACS Nano* **2021**, *15*, 15285–15293.
[62] B. Zhang, M. T. Trinh, B. Fowler, M. Ball, Q. Xu, F. Ng, M. L. Steigerwald, X. Y. Zhu, C. Nuckolls, Y. Zhong, *J. Am. Chem. Soc.* **2016**, *138*, 16426–16431.
[63] M. Ball, Y. Zhong, B. Fowler, B. Zhang, P. Li, G. Etkin, D. W. Paley, J. Decatur, A. K. Dalsania, H. Li, S. Xiao, F. Ng, M. L. Steigerwald, C. Nuckolls, *J. Am. Chem. Soc.* **2016**, *138*, 12861–12867.
[64] D. M. Guldi, B. M. Illescas, C. M. Atienza, M. Wielopolski, N. Martin, *Chem. Soc. Rev.* **2009**, *38*, 1587–1597.
[65] R. Ganesamoorthy, G. Sathiyan, P. Sakthivel, *Sol. Energy Mater. Sol. Cells* **2017**, *161*, 102–148.
[66] C. Brouillac, F. Lucas, D. Tondelier, J. Rault-Berthelot, C. Lebreton, E. Jacques, C. Quinton, C. Poriel, *Adv. Opt. Mater.* **2023**, *11*, 2202191.
[67] L. Hu, Y. Guo, X. Yan, H. Zeng, J. Zhou, *Phys. Lett. A* **2017**, *381*, 2107–2111.
[68] S. Canola, C. Graham, A. J. Perez-Jimenez, J. C. Sancho-Garcia, F. Negri, *Phys. Chem. Chem. Phys.* **2019**, *21*, 2057–2068.
[69] O. Koçak, I. P. Duru, I. Yavuz, *Adv. Theory Simul.* **2019**, *2*, 1800194.
[70] A. C. Grimsdale, K. L. Chan, R. E. Martin, P. G. Jokisz, A. B. Holmes, *Chem. Rev.* **2009**, *109*, 897–1091.
[71] X. Yang, X. Xu, G. Zhou, *J. Mater. Chem. C* **2015**, *3*, 913–944.
[72] L. Sicard, C. Quinton, J.-D. Peltier, D. Tondelier, B. Geffroy, U. Biapo, R. Métivier, O. Jeannin, J. Rault-Berthelot, C. Poriel, *Chem. Eur. J.* **2017**, *23*, 7719–7723.
[73] C. Poriel, J. Rault-Berthelot, *Chem. Soc. Rev.* **2023**, *52*, 6754–6805.
[74] C. Poriel, J. Rault-Berthelot, *Adv. Funct. Mater.* **2020**, *30*, 1910040.
[75] E. Kayahara, R. Qu, M. Kojima, T. Iwamoto, T. Suzuki, S. Yamago, *Chem. Eur. J.* **2015**, *21*, 18939–18943.
[76] P. Li, T. J. Sisto, E. R. Darzi, R. Jasti, *Org. Lett.* **2014**, *16*, 182–185.
[77] P. Li, B. M. Wong, L. N. Zakharov, R. Jasti, *Org. Lett.* **2016**, *18*, 1574–1577.
[78] M. Pena-Alvarez, L. Qiu, M. Taravillo, V. G. Baonza, M. C. Delgado, S. Yamago, R. Jasti, J. T. Navarrete, J. Casado, M. Kertesz, *Phys. Chem. Chem. Phys.* **2016**, *18*, 11683–11692.
[79] P. Ledwon, *Org. Electron.* **2019**, *75*, 105422.
[80] Y. Kuroda, Y. Sakamoto, T. Suzuki, E. Kayahara, S. Yamago, *J. Org. Chem.* **2016**, *81*, 3356–3363.
[81] F. Lucas, C. Brouillac, S. Fall, N. Zimmerman, D. Tondelier, B. Geffroy, N. Leclerc, T. Heiser, C. Lebreton, E. Jacques, C. Quinton, J. Rault-Berthelot, C. Poriel, *Chem. Mater.* **2022**, *34*, 8345–8355.
[82] F. Lucas, C. Quinton, S. Fall, T. Heiser, D. Tondelier, B. Geffroy, N. Leclerc, J. Rault-Berthelot, C. Poriel, *J. Mater. Chem. C* **2020**, *8*, 16354–16367.
[83] M. Fujitsuka, C. Lu, T. Iwamoto, E. Kayahara, S. Yamago, T. Majima, *J. Phys. Chem. A* **2014**, *118*, 4527–4532.
[84] J. Liu, L. Adamska, S. K. Doorn, S. Tretiak, *Phys. Chem. Chem. Phys.* **2015**, *17*, 14613–14622.
[85] D. A. Hines, E. R. Darzi, E. S. Hirst, R. Jasti, P. V. Kamat, *J. Phys. Chem. A* **2015**, *119*, 8083–8089.
[86] D. A. Hines, E. R. Darzi, R. Jasti, P. V. Kamat, *J. Phys. Chem. A* **2014**, *118*, 1595–1600.
[87] H. Shudo, M. Kuwayama, M. Shimasaki, T. Nishihara, Y. Takeda, N. Mitoma, T. Kuwabara, A. Yagi, Y. Segawa, K. Itami, *Nat. Commun.* **2022**, *13*, 3713.
[88] F. Lucas, D. Tondelier, B. Geffroy, T. Heiser, O. A. Ibraikulov, C. Quinton, C. Brouillac, N. Leclerc, J. Rault-Berthelot, C. Poriel, *Mater. Chem. Front.* **2021**, *5*, 8066–8077.
[89] C. Poriel, J. Rault-Berthelot, *Acc. Mater. Res.* **2023**, *3*, 379–390.
[90] P. Tourneur, F. Lucas, C. Brouillac, C. Quinton, R. Lazzaroni, Y. Olivier, P. Viville, C. Poriel, J. Cornil, *Adv. Photonics Res.* **2022**, *3*, 2200124.
[91] Z. Xu, B. Z. Tang, Y. Wang, D. Ma, *J. Mater. Chem. C* **2020**, *8*, 2614–2642.
[92] J. R. Sheats, H. Antoniadis, M. Hueschen, W. Leonard, J. Miller, R. Moon, D. Roitman, A. Stocking, *Science* **1996**, *273*, 884–888.
[93] R. H. Friend, R. W. Gymer, A. B. Holmes, J. H. Burroughes, R. N. Marks, C. Taliani, D. D. C. Bradley, D. A. D. Santos, J. L. Brédas, M. Lögdlund, W. R. Salaneck, *Nature* **1999**, *397*, 121–128.
[94] Y. Tao, C. Yang, J. Qin, *Chem. Soc. Rev.* **2011**, *40*, 2943–2970.
[95] M. A. Baldo, D. F. O'Brien, Y. You, A. Shoustikov, S. Sibley, M. E. Thompson, S. R. Forrest, *Nature* **1998**, *395*, 151–154.
[96] K. S. Yook, J. Y. Lee, *Adv. Mater.* **2014**, *26*, 4218–4233.
[97] Y. Wang, J. H. Yun, L. Wang, J. Y. Lee, *Adv. Funct. Mater.* **2021**, *31*, 2008332.
[98] C. Poriel, J. Rault-Berthelot, *Acc. Mater. Res.* **2022**, *3*, 379–390.
[99] C. Poriel, J. Rault-Berthelot, *Adv. Funct. Mater.* **2021**, *31*, 2010547.
[100] Y.-Z. Shi, H. Wu, K. Wang, J. Yu, X.-M. Ou, X.-H. Zhang, *Chem. Sci.* **2022**, *13*, 3625–3651.
[101] Y. Xiao, H. Wang, Z. Xie, M. Shen, R. Huang, Y. Miao, G. Liu, T. Yu, W. Huang, *Chem. Sci.* **2022**, *13*, 8906–8923.
[102] A. Endo, M. Ogasawara, A. Takahashi, D. Yokoyama, Y. Kato, C. Adachi, *Adv. Mater.* **2009**, *21*, 4802–4806.
[103] M. Y. Wong, E. Zysman-Colman, *Adv. Mater.* **2017**, *29*, 1605444.

© 2024 The Authors. Angewandte Chemie International Edition published by Wiley-VCH GmbH

15213773, 0, Downloaded from https://onlinelibrary.wiley.com/doi/10.1002/anie.202402608 by Université De Rennes, Wiley Online Library on [08/07/2024]. See the Terms and Conditions (https://onlinelibrary.wiley.com/terms-and-conditions) on Wiley Online Library for rules of use; OA articles are governed by the applicable Creative Commons License

[104] G. Méhes, H. Nomura, Q. Zhang, T. Nakagawa, C. Adachi, *Angew. Chem. Int. Ed.* **2012**, *51*, 11311–11315.
[105] J.-M. Teng, Y.-F. Wang, C.-F. Chen, *J. Mater. Chem. C* **2020**, *8*, 11340–11353.
[106] C.-C. Peng, S.-Y. Yang, H.-C. Li, G.-H. Xie, L.-S. Cui, S.-N. Zou, C. Poriel, Z.-Q. Jiang, L.-S. Liao, *Adv. Mater.* **2020**, *32*, 2003885.
[107] Y. Im, M. Kim, Y. J. Cho, J.-A. Seo, K. S. Yook, J. Y. Lee, *Chem. Mater.* **2017**, *29*, 1946–1963.
[108] C. Graham, M. Moral, L. Muccioli, Y. Olivier, Á. J. Pérez-Jiménez, J. C. Sancho-García, *Int. J. Quantum Chem.* **2017**, *118*, e25562.
[109] D. Chen, Y. Wada, Y. Kusakabe, L. Sun, E. Kayahara, K. Suzuki, H. Tanaka, S. Yamago, H. Kaji, E. Zysman-Colman, *Org. Lett.* **2023**, *25*, 998–1002.
[110] S. M. McAfee, G. C. Welch, *Chem. Rec.* **2019**, *19*, 989–1007.
[111] G. Zhang, J. Zhao, P. C. Y. Chow, K. Jiang, J. Zhang, Z. Zhu, J. Zhang, F. Huang, H. Yan, *Chem. Rev.* **2018**, *118*, 3447–3507.
[112] Y. Zhang, Y. Wang, C. Gao, Z. Ni, X. Zhang, W. Hu, H. Dong, *Chem. Soc. Rev.* **2023**, *52*, 1331–1381.
[113] Y. Lin, X. Zhan, *Acc. Chem. Res.* **2016**, *49*, 175–183.
[114] C. Xu, Z. Zhao, K. Yang, L. Niu, X. Ma, Z. Zhou, X. Zhang, F. Zhang, *J. Mater. Chem. A* **2022**, *10*, 6291–6329.
[115] D. Luo, W. Jang, D. D. Babu, M. S. Kim, D. H. Wang, A. K. K. Kyaw, *J. Mater. Chem. A* **2022**, *10*, 3255–3295.
[116] M. L. Ball, B. Zhang, Q. Xu, D. W. Paley, V. C. Ritter, F. Ng, M. L. Steigerwald, C. Nuckolls, *J. Am. Chem. Soc.* **2018**, *140*, 10135–10139.
[117] S. Hitosugi, K. Ohkubo, R. Iizuka, Y. Kawashima, K. Nakamura, S. Sato, H. Kono, S. Fukuzumi, H. Isobe, *Org. Lett.* **2014**, *16*, 3352–3355.
[118] D. Lu, G. Zhuang, H. Wu, S. Wang, S. Yang, P. Du, *Angew. Chem. Int. Ed.* **2017**, *56*, 158–162.
[119] Y. Xu, S. Gsänger, M. B. Minameyer, I. Imaz, D. Maspoch, O. Shyshov, F. Schwer, X. Ribas, T. Drewello, B. Meyer, M. von Delius, *J. Am. Chem. Soc.* **2019**, *141*, 18500–18507.
[120] C. Zhao, H. Meng, M. Nie, X. Wang, Z. Cai, T. Chen, D. Wang, C. Wang, T. Wang, *J. Phys. Chem. C* **2019**, *123*, 12514–12520.
[121] Y. Yang, S. Huangfu, S. Sato, M. Juricek, *Org. Lett.* **2021**, *23*, 7943–7948.
[122] Z. Sun, K. Li, Z. Xu, H. Deng, Z. Zhou, Y. Dang, *Angew. Chem. Int. Ed.* **2021**, *60*, 7649–7653.
[123] G. George, O. A. Stasyuk, A. Voityuk, A. J. Stasyuk, M. Solà, *Nanoscale* **2023**, *15*, 1221–1229.
[124] M. Freiberger, M. B. Minameyer, I. Solymosi, S. Fruhwald, M. Krug, Y. Xu, A. Hirsch, T. Clark, D. M. Guldi, M. von Delius, K. Amsharov, A. Gorling, M. E. Perez-Ojeda, T. Drewello, *Chem. Eur. J.* **2023**, *29*, e202203734.
[125] Y. Tang, J. Li, P. Du, H. Zhang, C. Zheng, H. Lin, X. Du, S. Tao, *Org. Electron.* **2020**, *83*, 105747.
[126] V. Coropceanu, J. Cornil, D. A. da Silva Filho, Y. Olivier, R. Silbey, J.-L. Brédas, *Chem. Rev.* **2007**, *107*, 926–952.
[127] E. Kayahara, L. Sun, H. Onishi, K. Suzuki, T. Fukushima, A. Sawada, H. Kaji, S. Yamago, *J. Am. Chem. Soc.* **2017**, *139*, 18480–18483.
[128] F. Lucas, L. Sicard, O. Jeannin, J. Rault-Berthelot, E. Jacques, C. Quinton, C. Poriel, *Chem. Eur. J.* **2019**, *25*, 7740–7748.
[129] F. Lucas, N. McIntosh, E. Jacques, C. Lebreton, B. Heinrich, B. Donnio, O. Jeannin, J. Rault-Berthelot, C. Quinton, J. Cornil, C. Poriel, *J. Am. Chem. Soc.* **2021**, *143*, 8804–8820.
[130] B. Xu, E. Sheibani, P. Liu, J. Zhang, H. Tian, N. Vlachopoulos, G. Boschloo, L. Kloo, A. Hagfeldt, L. Sun, *Adv. Mater.* **2014**, *26*, 6629–6634.
[131] L. Gao, T. H. Schloemer, F. Zhang, X. Chen, C. Xiao, K. Zhu, A. Sellinger, *ACS Appl. Energ. Mater.* **2020**, *3*, 4492–4498.
[132] R. K. Konidena, K. R. J. Thomas, J. W. Park, *ChemPhotoChem* **2022**, *6*, e202200059.
[133] C. Quinton, S. Thiery, O. Jeannin, D. Tondelier, B. Geffroy, E. Jacques, J. Rault-Berthelot, C. Poriel, *ACS Appl. Mater. Interfaces* **2017**, *9*, 6194–6206.
[134] S. Wang, X. Li, G. Zhuang, M. Chen, P. Huang, S. Yang, P. Du, *Chem. Commun.* **2021**, *57*, 9104–9107.
[135] S. Wang, X. Li, K. Wei, X. Zhang, S. Yang, G. Zhuang, P. Du, *Eur. J. Org. Chem.* **2022**, e202101493.
[136] Y. Lv, J. Lin, K. Song, X. Song, H. Zang, Y. Zang, D. Zhu, *Sci. Adv.* **2021**, *7*, eabk3095.
[137] J. Lin, S. Wang, F. Zhang, B. Yang, P. Du, C. Chen, Y. Zang, D. Zhu, *Sci. Adv.* **2022**, *8*, eade4692.
[138] C. Brouillac, N. McIntosh, B. Heinrich, O. Jeannin, O. De Sagazan, N. Coulon, J. Rault-Berthelot, J. Cornil, E. Jacques, C. Quinton, C. Poriel, *Adv. Sci.* **2024**, *11*, 2309115.
[139] J. H. Griwatz, M. L. Kessler, H. A. Wegner, *Chem. Eur. J.* **2023**, *29*, e202302173.
[140] Y. Yoshigoe, Y. Tanji, Y. Hata, K. Osakada, S. Saito, E. Kayahara, S. Yamago, Y. Tsuchido, H. Kawai, *JACS Au* **2022**, *8*, 1857–1868.
[141] M. Hermann, D. Wassy, B. Esser, *Angew. Chem. Int. Ed.* **2021**, *60*, 15743–15766.
[142] T. C. Lovell, K. G. Fosnacht, C. E. Colwell, R. Jasti, *Chem. Sci.* **2020**, *11*, 12029–12035.
[143] D. Ari, E. Dureau, O. Jeannin, J. Rault-Berthelot, C. Poriel, C. Quinton, *Chem. Commun.* **2023**. *59*, 14835–14838.
[144] V. B. R. Pedersen, T. W. Price, N. Kofod, L. N. Zakharov, B. W. Laursen, R. Jasti, M. B. Nielsen, *Chem. Eur. J.* **2023**, *30*, e202303490.
[145] J.-D. Peltier, B. Heinrich, B. Donnio, J. Rault-Berthelot, E. Jacques, C. Poriel, *ACS Appl. Mater. Interfaces* **2017**, *9*, 8219–8232.
[146] S. Bebiche, P. A. Cisneros-Perez, T. Mohammed-Brahim, M. Harnois, J. Rault-Berthelot, C. Poriel, E. Jacques, *Mater. Chem. Front.* **2018**, *2*, 1631–1641.
[147] H. Usta, A. Facchetti, T. J. Marks, *Acc. Chem. Res.* **2011**, *44*, 501–510.
[148] H. Usta, A. Facchetti, T. J. Marks, *J. Am. Chem. Soc.* **2008**, *130*, 8580–8581.
[149] P. Seitz, M. Bhosale, L. Rzesny, A. Uhlmann, J. S. Wossner, R. Wessling, B. Esser, *Angew. Chem. Int. Ed.* **2023**, *62*, e202306184.
[150] S. Wang, F. Chen, G. Zhuang, K. Wei, T. Chen, X. Zhang, C. Chen, P. Du, *Nano Res.* **2023**, *16*, 10342–10.

Manuscript received: February 5, 2024
Accepted manuscript online: May 14, 2024
Version of record online: ■■, ■■

© 2024 The Authors. Angewandte Chemie International Edition published by Wiley-VCH GmbH

15213773, 0, Downloaded from https://onlinelibrary.wiley.com/doi/10.1002/anie.202402608 by Université De Rennes, Wiley Online Library on [08/07/2024]. See the Terms and Conditions (https://onlinelibrary.wiley.com/terms-and-conditions) on Wiley Online Library for rules of use; OA articles are governed by the applicable Creative Commons License

Reviews

Cycloparaphenylenes

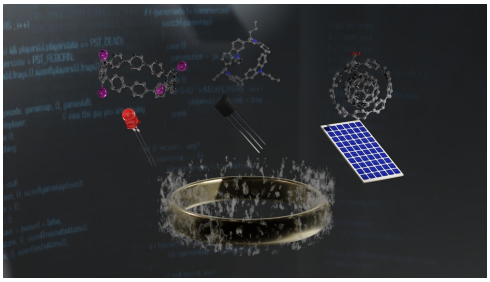

The different nanohoops used to date in organic electronics are described in this Review. Through a structure-properties relationship study, the different performances reached are analysed and the potential of this new generation of curved materials discussed. This Review aims to stimulate future molecular designs of functional materials based on these conjugated macrocycles.

© 2024 The Authors. Angewandte Chemie International Edition published by Wiley-VCH GmbH

15213773, 0, Downloaded from https://onlinelibrary.wiley.com/doi/10.1002/anie.202402608 by Université De Rennes, Wiley Online Library on [08/07/2024]. See the Terms and Conditions (https://onlinelibrary.wiley.com/terms-and-conditions) on Wiley Online Library for rules of use; OA articles are governed by the applicable Creative Commons License